University of South Bohemia in České Budějovice

Faculty of Science

Bachelor thesis

The novel kinetoplastid kinesin TbKIFx and its partner TbPH1 are associated with specific cytoskeletal structures of *Trypanosoma brucei*

Faculty of Science, University of South Bohemia

Institute of Parasitology, Biology Centre, Czech Academy of Sciences

Nora Müller

2019

Supervised by doc. Hassan Hashimi, Ph.D.

České Budějovice 2019

Müller N., 2019: The novel kinetoplastid kinesin TbKIFx and its partner TbPH1 are associated with specific cytoskeletal structures of *Trypanosoma brucei*. Bc. Thesis, in English – 47 p, Faculty of Science, University of South Bohemia, České Budějovice, Czech Republic.

Annotation

This study focuses on the kinesin motor protein TbKIFx and its presumably catalytically inactive partner TbPH1 in *Trypanosoma brucei*. Not much is known about the TbPH1/TbKIFx dimer so far. The aim of our research was to localize TbKIFx/TbPH1 in procyclic and bloodstream cells and to investigate potential cargo candidates. We believe that we identified the microtubule quartet and mature basal body as potential binding sites of TbKIFx/TbPH1 in both life cycle stages of *T. brucei*. However, our investigations into tyrosine-phosphorylated proteins as possible cargo of TbKIFx/TbPH1 remain inconclusive.

Declaration

I hereby declare that I have worked on my bachelor's thesis independently and used only the sources listed in the bibliography.

I hereby declare that, in accordance with Article 47b of Act No. 111/1998 in the valid wording, I agree with the publication of my bachelor thesis, in full to be kept in the Faculty of Science archive, in electronic form in publicly accessible part of the STAG database operated by the University of South Bohemia in České Budějovice accessible through its web pages. Further, I agree to the electronic publication of the comments of my supervisor and thesis opponents and the record of the proceedings and results of the thesis defense in accordance with aforementioned Act No. 111/1998. I also agree to the comparison of the text of my thesis with the Theses.cz thesis database operated by the National Registry of University Theses and a plagiarism detection system.

České Budějovice, 11.12.2019

.....

Nora Müller

Acknowledgments

I would first like to thank my supervisor Hassan Hashimi, who welcomed me with open arms in his team. He always believed in my abilities and gave me strength, motivation and encouragement during my work in the laboratory. Further, he taught me to be patient, cooperative and to be considerate of other colleagues, which are essential features for further work in the scientific field. His support, constructive comments and professional advice guided me through my working time and helped me to accomplish several objectives of the project.

Special thanks also to the whole MICOS-team, in particular, Iosif Kaurov and Jirka Heller. They were always open to questions and offered help, whenever I needed. Especially during the first few months, they patiently introduced me in experimental procedures and techniques but also provided valuable advice throughout my whole time in Budweis.

I would like to acknowledge Julius Lukeš for giving me the opportunity to work in his laboratory and therefore on my thesis.

Moreover, I am grateful to all members of the Lab of Functional Biology of Protists. Many of them provided me personal and professional guidance and made my stay even more enjoyable.

Finally, I must express my very profound gratitude to my parents, who provided me with unfailing support and love throughout my whole study. Thank you.

Abstract

Kinesins are evolutionarily conserved motor proteins that fulfil multiple functions in various cellular processes. *Trypanosoma brucei* lack many homologues of conserved kinesins, but also possess several trypanosome-specific kinesins of unknown functions. These include TbKIFx, which is partnered with a putatively catalytically inactive kinesin-like protein named TbPH1. Their interaction persists under high ionic strength conditions. The cytoskeleton of *T. brucei* exhibits some unique features as well, which are not shared by other eukaryotic representatives. For instance, the subpellicular microtubule-corset, which determines the cell shape of trypanosomes, and the microtubule quartet (MtQ), which originates between the basal bodies (BBs) and runs along the flagellum attachment zone (FAZ).

In this study, we have identified the potential location of TbKIFx/TbPH1 in isolated cytoskeletons of bloodstream and procyclic stage *T. brucei* by immunofluorescence assays (IFA) and scanning electron microscopy (SEM). TbKIFx is enriched with the FAZ and mature basal body (mBB) in bloodstream stage *T. brucei*, indicating a possible interaction with the MtQ. This hypothesis is further strengthened by investigations of procyclic stage *T. brucei*, showing a co-localization of TbPH1 with the mBB and MtQ. Interestingly, cytoskeleton-associated tyrosine-phosphorylated proteins also overlap with TbKIFx in bloodstream cells, suggesting their interaction with the pleckstrin homology domain of TbPH1. Based on the obtained results, we conclude that TbKIFx/TbPH1 may interact with tyrosine-phosphorylated proteins, perhaps carrying them along the MtQ.

Table of Content

Abbreviations

APS - Ammonium persulfate
ATP - Adenosine triphosphate
BBs – Basal bodies
BioID - Biotin identification
DAPI - 4′,6-diamidino-2-phenylindole
DMSO - Dimethyl sulfoxide
DNA - Deoxyribonucleic acid
dNTP - Deoxyribonucleotide triphosphate
EDTA - Ethylenediaminetetraacetic acid
EGTA - Egtazic acid
ER - Endoplasmic reticulum
FAZ - Flagellum attachment zone
FP - Flagellar pocket
GTP - Guanosine triphosphate
HD - Homeodomain
HF - High fidelity
IFA - Immunofluorescence assay
KIFs - Kinesins
LDS - Lithium dodecyl sulfate
MAPs - Microtubule-associated proteins
mBB – Mature basal body
mRNA - Messenger ribonucleic acid
MtQ - Microtubules quartet
PB - Phosphate buffer without salt
pBB – Pro-basal body
PBS - Phosphate Buffered Saline
PCR - Polymerase chain reaction
PFA - Paraformaldehyde
PFR - Paraflagellar rod
PH - Pleckstrin homology
PIPES - Piperazine-N,N′-bis(2-ethanesulfonic acid)
p-Tyr - Tyrosine-phosphorylated proteins
RNA - Ribonucleic acid
RNAi - Ribonucleic acid interference
SDS - Sodium dodecyl sulfate
SEM - Scanning electron microscopy
STED – Stimulated emission depletion
TAC - Tripartite attachment complex
TAE - Tris-acetate-EDTA
TBS - Tris-buffered saline
TEM - Transmission electron microscopy
TEMED - Tetramethylethylenediamine
Tris – Trisaminomethane
WD – Working distance

1. Introduction

1.1. *Trypanosoma brucei*

Trypanosomes are unicellular flagellated protozoan parasites, which belong to the class Kinetoplastea (Balmer *et al.*, 2011; Adl *et al.*, 2018). Kinetoplastea are part of the Discoba, an early branching clade (Figure 1), therefore making trypanosomes an excellent organism for evolutionary cell biology (Hampl *et al.*, 2009; Lynch *et al.*, 2014; Adl *et al.*, 2018). *Trypanosoma brucei*, a species of trypanosomes, represents an ideal system for studying morphology, organelle positioning, cell division, protein trafficking and various other aspects of cell biology (Matthews, 2005).

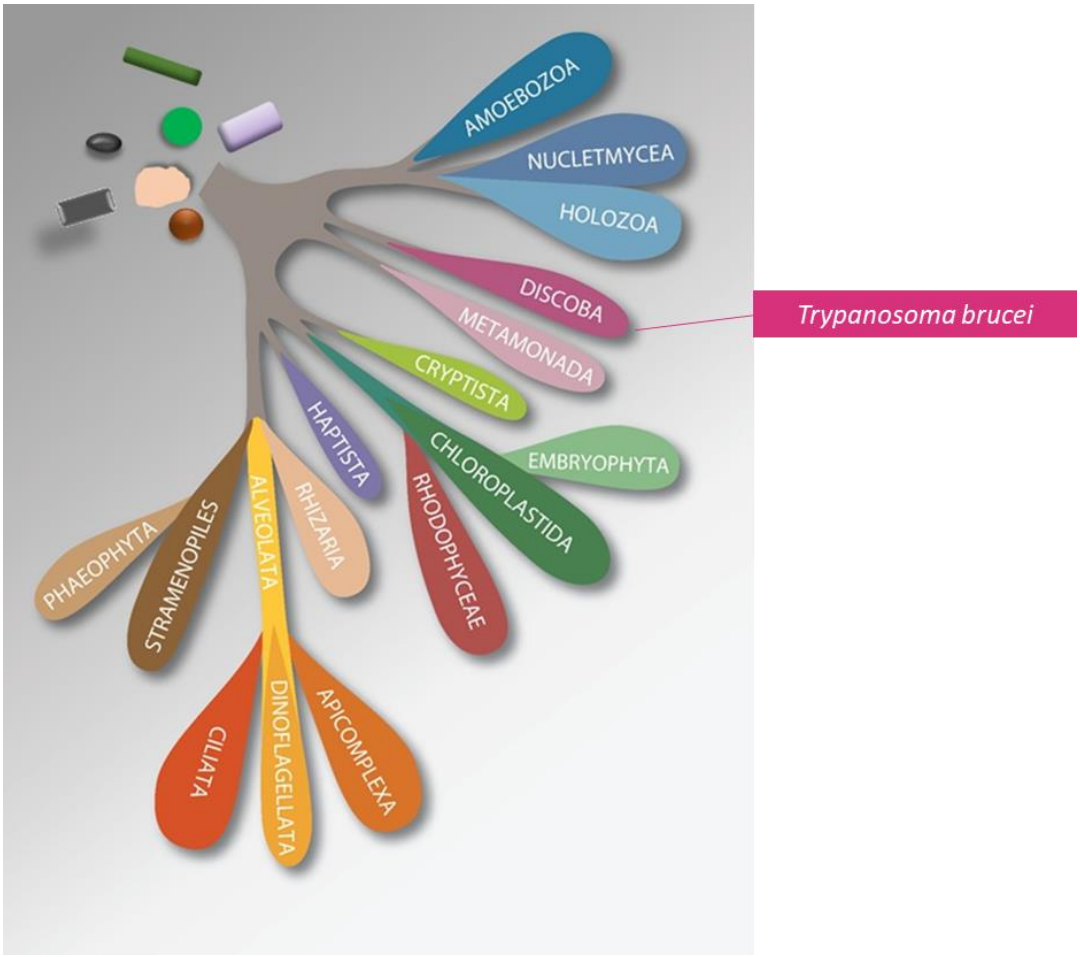

Figure 1: Diversity of eukaryotic protists. Trypanosoma belong to the Discoba clade. Adapted from Adl *et al.*, 2018.

T. brucei possess many distinct life cycle stages, which allow it to master diverse environments with different nutrients (Matthews, 2005). In mammalian hosts, *T. brucei* exist in two different forms, the proliferative long-slender and short-stumpy bloodstream form. Within the tsetse fly, *T. brucei* are concentrated in two different locations as three major forms: the procyclic

form established within the midgut, and the epimastigote and metacyclic trypomastigotes located in the salivary gland.

In the laboratory, two proliferating life stages are regularly used as they can be easily cultured *in vitro*: the long slender bloodstream form and the procyclic form (Montagnes *et al.*, 2012).

1.2. Cytoskeletal Architecture of *Trypanosoma brucei*

The cell body of *T. brucei* is enclosed by a helical array of subpellicular microtubules arranged along the cell axis, which are in close contact with the overlying cell membrane (Hemphill *et al.*, 1991; Kohl & Gull, 1998). The link between microtubules and the cell membrane, as well the links between adjacent microtubules, are mediated by microtubule-associated proteins (MAPs) (Schneider *et al*., 1988; Kohl & Gull, 1998). Microtubules are composed of protofilaments containing repeated αβ-tubulin heterodimers, which result in the characteristic polarity of microtubules having their positive ends towards the posterior of the cell (Kohl & Gull, 1998).

T. brucei possess a single flagellum, which is anchored in the cytoplasm by the basal body and exits the cytoplasm through the flagellar pocket (FP), whereupon it runs along most of the cell length (Figure 2) (Langousis & Hill, 2014; Field & Carrington, 2009; Sunter & Gull, 2016). The flagellum is composed of 9+2 axoneme and the paraflagellar rod (PFR), which is vital for motility (Vaughan *et al.*, 2008).

Flagellum attachment is accomplished by junctional complexes, which tightly link the flagellum membrane and plasma membrane utilizing proteins in the flagellum and the cell body. These junctional complexes represent the so-called flagellum attachment zone (FAZ) (Figure 3) (Langousis & Hill, 2014). FAZ comprises of FAZ filaments and the associated microtubule quartet (MtQ) that is closely associated with the endoplasmic reticulum (ER) (Figure 3) (Kohl *et al.*, 1999; Lacomble *et al.*, 2012).

The FAZ filaments are cytoplasmic and are connected to the axoneme and PFR of the flagellum (Figure 3) (Ralston & Hill, 2008; Langousis & Hill, 2014). The FAZ filaments originate just anterior to the flagellar pocket (Figure 2) and are located within a gap between subpellicular microtubules and the MtQ (Figure 3), which it joins to the anterior end of the cell (Langousis & Hill, 2014; Vaughan *et al.*, 2008).

The MtQ is a sub-set of subpellicular microtubules, that has its minus end at the posterior end of the cell (Höög *et al.*, 2012; Sunter & Gull, 2016). This contrasts the polarity of the other subpellicular microtubules creating an asymmetric seam within the microtubule corset (Figure 3) (Sunter & Gull, 2016). The MtQ originates between the mature basal body (mBB) and the

pro-basal body (pBB) and wraps around the flagellar pocket before following the FAZ filaments along the cell axis (Figure 2) (Vaughan & Gull, 2015; Vaughan *et al.*, 2008). To date, the MtQ remains poorly understood. Only the sperm flagellar protein1 (TbSpef1) has been localized to the MtQ, which is found between the basal bodies (BBs) and the Bi-lobe (Figure 2) (Gheiratmand *et al.*, 2012). Spef1 was initially identified in chordates appearing to be involved in sperm flagellum (Chan *et al.*, 2005). The maintenance of the Spef1 throughout evolution suggests that the protein plays an essential part of the flagellar structure.

The basal bodies (BBs) are positioned at the base of the FP (Vaughan & Gull, 2015). The mature basal body (mBB) is linked to the kinetoplast and the FP (Vaughan & Gull, 2015; Trikin *et al.*, 2016). The link between the kinetoplast and the mature basal body is mediated by a set of filaments, the tripartite attachment complex (TAC) (Trikin *et al.*, 2016). The mBB acts as base for the assembled flagellum and anchors it in the cytoplasm at the posterior of the cell (Vaughan & Gull, 2015; Field & Carrington, 2009). The adjacent pro-basal body (pBB) forms the new flagellum during cell division (Vaughan *et al.*, 2008). The pBB is as well physically connected to the kinetoplast by TAC (Trikin *et al.*, 2016). However, the TAC connecting the pBB and the kinetoplast misses the protein TAC102, which is essential for mitochondrial genome segregation. The pBB is also linked to the MtQ through fine filaments, which were quite recently discovered (Vaughan & Gull, 2015).

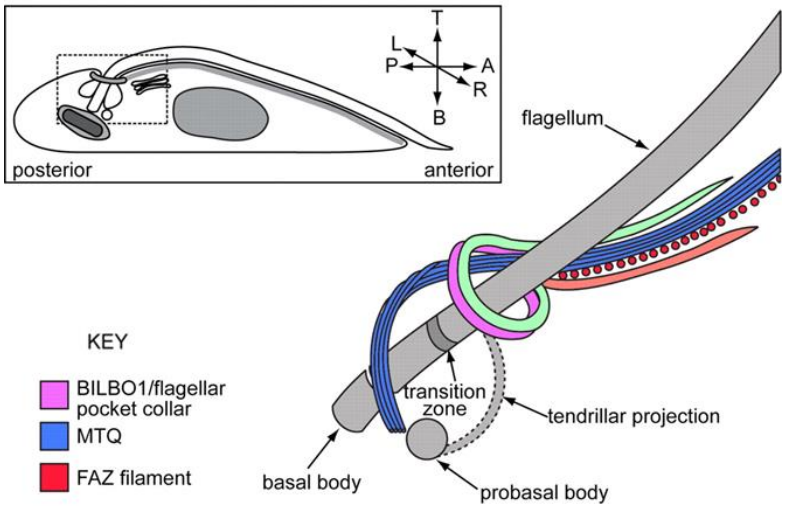

Figure 2: Morphological model of the microtubule quartet (MTQ), basal bodies (BBs) and flagellum attachment zone (FAZ) assembly. The MtQ originates between the mature basal body (mBB) and pro-basal body (pBB) and wraps around the flagellar pocket (FP) before forming an asymmetric seam with the FAZ along the whole cell body. Taken from Esson *et al.*, 2012.

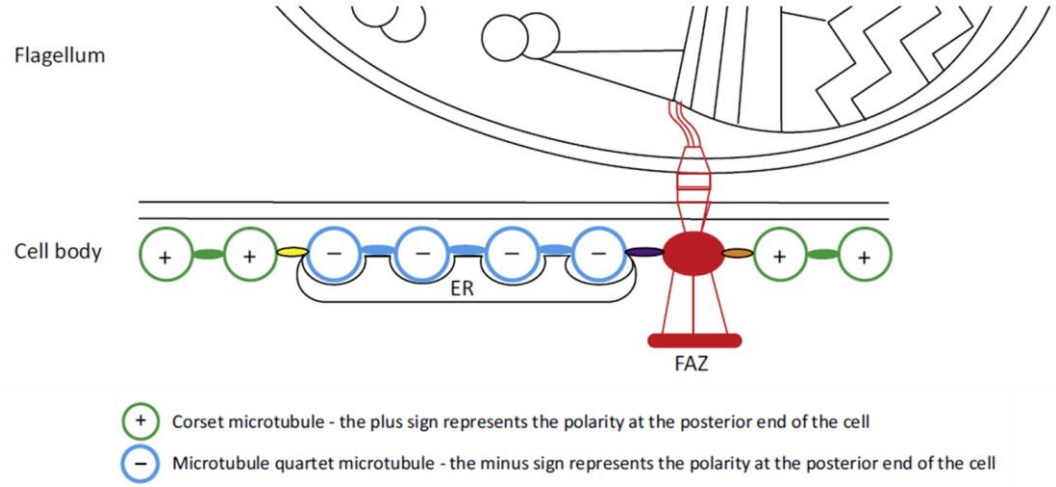

Figure 3: Sketch of the flagellum attachment zone (FAZ) assembly. The cytoplasmic FAZ filaments (red) are positioned within a gap between subpellicular microtubules (green circles) and the microtubule quartet (MtQ) (blue circles). The FAZ filaments are connected to the axoneme and paraflagellar rod (PFR) of the flagellum. The adjacent MtQ has its minus end at the posterior end of the cell. Therefore, the polarity of the MtQ contrasts the polarity of other subpellicular microtubules, which is indicated by the opposite sign (minus) in the picture. The MtQ is connected with the endoplasmic reticulum (ER). Taken from Sunter & Gull, 2016.

1.3. Kinesins

Fundamental cellular functions, survival, proliferation etc. are achieved by intracellular transport. The transport of various cargos, including membranous organelles, protein rafts and mRNAs, is realized by molecular motors. These motors are divided into three large superfamilies - kinesins, dyneins and myosins (Hirokawa *et al.*, 2009).

Kinesins (KIFs) are motor proteins, that move along microtubules to transport their cargo to the appropriate destination (Hirokawa *et al.*, 2009; Alberts *et al.*, 2002). A kinesin motor consists of a highly conserved kinesin motor domain, a unique stalk and tail domains, enabling the kinesins to dimerize and/or to bind to cargo or adaptor proteins (Figure 4) (Hirokawa *et al.*, 2009).

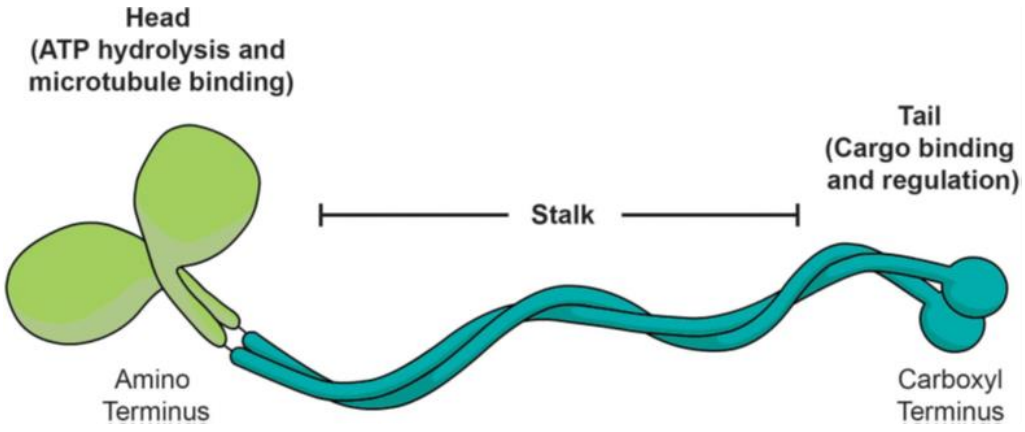

Figure 4: Generalized kinesin dimer structure. A kinesin consists of a head containing the catalytic motor domain and the microtubule-binding site, a unique stalk and a tail carrying the cargo. Taken from Lucanus & Yip, 2017.

The kinesin motor domain (so -called "head") hydrolyses ATP to cause conformational changes that generate motile force. The position of the head is either on the amino terminus (N-kinesins), in the middle (M-kinesins) or on the carboxyl terminus (C-kinesins). Depending on the position of the head, kinesins move in different directions. N-kinesins move as monomers or assembled as dimers towards the plus end-direction. C-kinesins move solely as dimers to the minus end-direction. And M-kinesins depolymerize microtubules (Hirokawa *et al.*, 2009; Sablin, 2000).

The catalytic core of the motor domain consists of an eight-stranded beta-sheet with three alpha helices on each side. The central beta-sheet contains the nucleotide binding cleft with the highly conserved P-loop motif (GXXXXGK[TS]), originally called the Walker A motif (Rice *et al.*, 1999; Saraste *et al.*, 1990). Upon the binding of ATP to the Walker A motif and its hydrolysis, switch I and II are set into motion. The rotation of switch II, together with its adjacent loops and helix, is proposed to control the interactions of the head with the adjacent neck. This results in the directional movement of the kinesin motor along the microtubules (Hirose *et al.*, 2006).

1.4. An odd pair: TbKIFx and TbPH1

TbKIFx, a member of the kinesin superfamily proteins, is a N-terminal microtubule motor restricted to kinetoplastids (Kaltenbrunner, 2017; Wickstead & Gull, 2006). Its coiled coil region (Figure 5) most likely enables to bind to the kinesin-like protein TbPH1, where their interaction withstands conditions of high ionic strength.

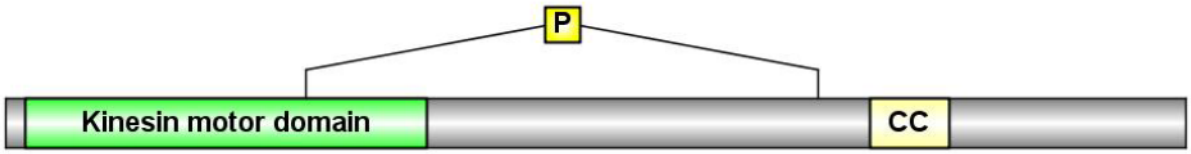

Figure 5: Structural features of TbKIFx. The kinesin features a kinesin motor domain and a coiled coil (CC) region enabling the interaction with TbPH1. P represents phosphorylation sites (P).

A large number of kinesin-like proteins are encoded in the trypanosome genome, some of still unknown function (Hu *et al.*, 2012). Among them is the kinesin-like protein TbPH1, which contains: a homeodomain (HD) -like sequence, a Pleckstrin homology (PH) domain, a coiled-coil region and a kinesin motor domain (Figure 6). A methylation resides at the conserved arginine-residue (R540) in the coiled-coil region and a phosphorylated serine at the beginning of the HD-like domain (Figure 6). The N-terminal motor domain probably enables TbPH1 to bind microtubules. However, a mutation in the Walker A motif ablates hydrolysis of ATP or GTP. Thus, TbPH1 is likely not a true motor protein (Kaltenbrunner, 2017).

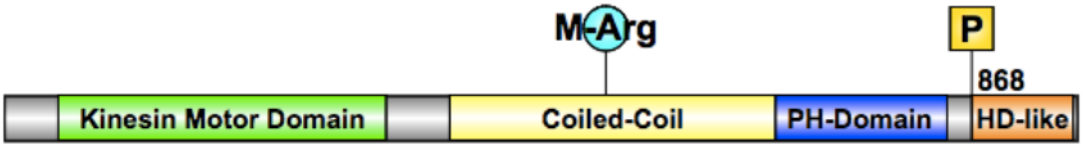

Figure 6: Structural composition of TbPH1. TbPH1 comprises of a kinesin motor domain with unfunctional Walker A motif, a coiled coil region enabling the interaction with TbKIFx, a Pleckstrin homology (PH) domain and a homeodomain (HD) -like domain. The coiled-coil region contains a methylation at the conserved arginine-residue (R540) (M-Arg) and a phosphorylated serine (P) at the beginning of the HD-like domain. Taken from Kaltenbrunner, 2017.

Not much is known about the proteins TbKIFx and TbPH1. In fact, only one study has laid the foundations for our research (Kaltenbrunner, 2017). Despite several attempts of localizing TbPH1 to cytoplasmic organelles as well as cytoskeletal structures of procyclic *T. brucei*, its distinct localization remained unclear. Also, function and potential cargos are still unknown. However, Kaltenbrunner (2017) indicated that the PH-domain of TbPH1 might determine its functionality.

1.5. Pleckstrin homology domain

PH domains are made up of approximately 100-120 amino acids (Lemmon *et al.*, 2001). They are present in a variety of modular proteins involved in signalling, cytoskeletal organization, membrane trafficking and phospholipid processing (Lemmon *et al*., 2001; Scheffzek & Welti, 2012). Moreover, PH domains are found in proteins expressed in animals (i.e. mammals, Drosophila etc.), protists and yeast, therefore indicating an early evolutionary origin in eukaryotes (Shaw, 1996). For instance, there are probably 252 different proteins containing at least one PH domain in the human genome, making it one of the most abundant domains (Lemmon *et al.*, 2001).

However, the PH amino acid alignment shows poorly conserved peptides interspersed with even less-well-conserved linker sequences (Shaw, 1996). Instead, they may only share the PH domain fold (Figure 7), thereby conceivably forming subclasses with different functions (Lemmon *et al.*, 2001). The PH fold may mediate phosphotyrosine and polyproline peptide binding to other signalling proteins, and phospholipid binding (Figure 7), which is proposed to be more exceptional than the protein-protein interactions (Scheffzek & Welti, 2012).

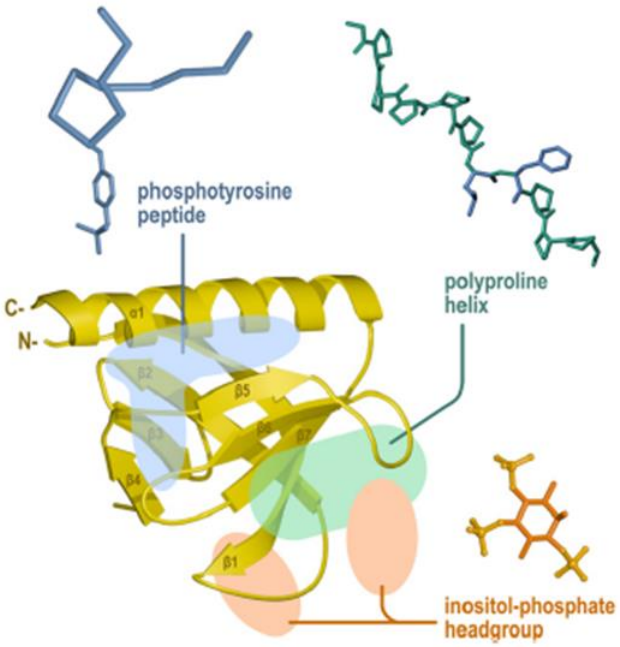

Figure 7: Pleckstrin homology (PH) domain and its diverse binding sites. The PH fold possesses binding sites for phosphotyrosine peptides (blue), polyproline helices (green) and phosphorylated inositol head groups (orange). Taken from Scheffzek & Welti, 2012.

2. Aims

The aims of the thesis were to:

I. Generate bloodstream *T. brucei* TbKIFx-V5 and TbPH1-HA cell lines

II. Generate bloodstream *T. brucei* RNAi-TbKIFx and RNAi-TbPH1 cell lines

III. Verify the interaction of TbKIFx and TbPH1 in bloodstream and procyclic form by immunofluorescence assays (IFA)

IV. Localize TbKIFx and TbPH1 to specific cytoskeletal structures of bloodstream and procyclic *T. brucei*, such as the basal body and the FAZ

V. Investigate the interaction of TbPH1 with tyrosine-phosphorylated proteins by IFA in bloodstream cells

VI. Investigate whether knockdown of TbPH1 affects tyrosine-phosphorylated proteins in procyclic cells by western blotting

3. Materials and Methods

3.1. Cultivation of *Trypanosoma brucei*

The long slender bloodstream form of *T. brucei* is cultivated in HMI-9 media containing 10% (v/v) fetal bovine serum and is incubated at 5% CO_2 and 37 °C (Hirumi & Hirumi, 1989). The bloodstream cell line SmOx B4, used for experiments, was grown in media containing 0.1 µg mL^{-1} puromycin, maintaining the SmOx transgenic construct containing genes for T7 RNA polymerase and the tetracycline repressor (Poon *et al.*, 2012). Upon *in situ* tagging of the desired proteins, specific drugs were used for selecting the respective cell lines (Table I).

Table I: Generated bloodstream cell lines and the corresponding selective drugs.

Cell line (Bloodstream form)	Selective drug	Selective drug / µg mL^{-1}
TbPH1-HA	Puromycin Neomycin	0.10 2.50
TbPH1-HA and TbKIFx-V5	Puromycin Neomycin Hygromycin	0.10 2.50 1.00
TbPH1-HA and TbKIFx-V5 TbPH1-RNAi	Puromycin Neomycin Hygromycin Phleomycin	0.10 2.50 1.00 0.75
TbPH1-HA and TbKIFx-V5 TbKIFx-RNAi	Puromycin Neomycin Hygromycin Phleomycin	0.10 2.50 1.00 0.75

Procyclic *T. brucei* were cultivated in SDM-79 media supplemented with 10% (v/v) fetal bovine serum and 2.5 µg mL^{-1} hemin and incubated at 5% CO_2 and 27 °C (Brun & Schonenberger, 1979). The used procyclic cell lines were generated by MSc. Sabine Kaltenbrunner and grown with their respective selective drugs, where the parental cell line SmOx P9 served as control (Table II) (Poon *et al.*, 2012).

Table II: Used procyclic cell lines and corresponding selective drugs.

Cell line (Procyclic form)	Selective drug	Selective drug / µg mL^{-1}
SmOx P9	Puromycin	1.0
SmOx P9 TbPH1-HA and TbKIF-V5	Puromycin Neomycin Hygromycin	1.0 15 50
SmOx P9 TbPH1-HA and TbKIF-V5 TbKIF-RNAi	Puromycin Neomycin Hygromycin Phleomycin	1.0 15 50 2.5

For RNAi-induction in bloodstream and procyclic cell lines, 1 µg mL^{-1} doxycycline was supplemented to the media containing the appropriate selective drugs (Table I & II).

3.2. Gene tagging in *Trypanosoma brucei*

3.2.1. Long primer PCR

For generating DNA constructs for *in situ* tagging of the proteins of interest, we applied essentially the same method used by Dean *et al.* (2015) with small modifications. To mediate the amplification by polymerase chain reaction (PCR), 31 µL MiliQ H_2O were combined with 1 µL of pPOT (25 ng μL^{-1}), 0.2 mM dNTPs (New England Biolabs), 1% DMSO (New England Biolabs), 10 µL of 5x Q5 Reaction Buffer (New England Biolabs), 1 µL of Q5 HF polymerase (New England Biolabs), 1 µM forward primer and 1 µM reverse primer, yielding 50 µL PCR solution (Dean *et al.*, 2015). The negative control contained the same PCR mixture, except the plasmid (pPOT), thus precluding any amplification. The used plasmid was the modified pPOTv4 vector containing the V5 tag with hygromycin as a resistance marker, and the HA tag with a neomycin resistance marker (Kaurov *et al.*, 2018).

Previously designed primers were used for the PCR amplification of the TbKIFx-V5 and the TbPH1-HA DNA constructs (Table III) (Kaltenbrunner, 2017). The forward primers contain the last 80 nucleotides of the target open reading frame (excluding the stop codon) and the pPOT annealing sequence (lower case). The reverse primers consist of the reverse complement of the first 80 nucleotides of the target genes and the pPOT annealing sequence (lower case) (Dean *et al.*, 2015).

Table III: Primers for generating the TbPH1-HA and TbKIFx-V5 constructs.

Primer	Sequence (5'-3')
C-term. TbPH1-HA, FW	TTTCTTCCGGTCTTGACTTATTCCGCTCAGGGAAGCTTTATGATTTCTTA TGCGAAAAGAGAGTCATACCGCTCCCGTACggttctggtagtggttcc
C-term. TbPH1-HA, RV	ATAATAAAGAGGAAGGGAAGGTAAAGTTCAGAAACAAATTCTGTTGGC TCCTGATAACACTCTCATATTTCCTTCACCGCccaatttgagagacctgtgc
C-term. TbKIFx-V5, FW	AACTACAGTTGCAAATGTGCATGATAGGAAGAAGTTGCCTCACGATGG AGCGTTGGAAAGCGGAACATGTCGGAACCGCAggttctggtagtggttcc
C-term. TbKIFx-V5, RV	TTGCGCGTGGCTCTAATTCCTTCTTTGTGTTCCGTCACGCTAAACAAATA CCAGTTGTTGTTGTTGTTTTTTCTTTCTTTccaatttgagagacctgtgc

The PCR ran under the PCR conditions shown in Table IV, which were based on Dean *et al.* (2015).

Table IV: PCR parameters according to Dean *et al.* (2015). The cycle from denaturation to extension was repeated 25 times.

PCR-step	Temperature / °C	Time / s
Initialization	94	300
Denaturation	94	15
Annealing	65	30
Extension	72	120
Final elongation	72	420
Final hold	12	Indefinite

pTrypSon RNAi constructs (McAllaster *et al.*, 2016) for electroporation were already prepared (Kaltenbrunner, 2017). Thus, only the linearization of the constructs was performed using 3 µL high fidelity NotI (10,000 U mL^{-1}) (NEB) restriction enzyme for 10 µg DNA in a solution containing 10 µL of 10 x Cutsmart buffer (NEB) and 87 µL MiliQ H_2O, where the mixture was left overnight at 37 °C.

3.2.2. Verification

Both, PCR-products and the linearized RNAi-constructs, were verified using agarose gel electrophoresis. Agarose weighing 0.6 g was dissolved in 60 mL of 1x Tris-acetate-EDTA (TAE) buffer solution (40 mM Tris, 20 mM acetic acid and 1 mM EDTA), to yield an agarose gel percentage of 1% (w/v). The mixture was heated to dissolve the agarose and then cooled to approximately 50 °C before adding 50 µg of ethidium bromide (ThermoFisher). Thereafter, the solution was immediately poured into the gel tray of the gel electrophoresis apparatus and left to solidify. The solid gel was submerged in 1x TAE. A mixture, consisting of the DNA of interest and 1x glycerol DNA loading buffer (ThremoFisher), was subsequently added into the wells. For separation, a voltage of 100 V was applied until the bromophenol blue dye migrated towards the end of the gel. To verify the correct molecular weight of the constructs, the DNA was visualized using ChemiDoc XRS+ Imaging system run with Image Lab software (Bio-Rad).

3.2.3. Electroporation of bloodstream *Trypanosoma brucei*

Prior to the electroporation, the DNA construct was precipitated using 96% ethanol and 3 M sodium acetate (pH 5.2) and left in -20 °C for several hours. Then, the DNA was centrifuged at 4 °C for 15 min at 16,100 x g. The supernatant was discarded, and the DNA-pellet was left to dry. Meanwhile, approximately 5 x 10^7 bloodstream *T. brucei* cells were harvested by centrifugation at room temperature for 10 min at 1,300 x g to remove the media. Eventually, the DNA was resuspended in 100 µL of the electroporation solution at 4 °C containing 81.8 µL Human T-cell Nuceloefector solution and 18.2 µL Supplement 1 (Lonza) and used to resuspend the cell pellet. Upon resuspension, the mixture was transferred into a cuvette and electroporated using the Amaxa X-001 program (Lonza). Subsequently, the electroporated cells were diluted in 30 mL media (Tube A), from which 3 mL were further diluted in 30 mL (Tube B). This step was once more repeated using 3 mL from tube B to produce tube C. Finally, 1 mL aliquots of each dilution (A, B, C) were distributed on three 24 well plates and incubated at 5% CO_2 and 37 °C for approximately 16 h, whereon 1 mL of media containing double the normal concentration of selection drug was added. Transformed cells were usually detected on day 5 or 6 after induction.

3.2.4. Growth measurements

For examining the growth of *T. brucei* upon depletion of TbKIFx, growth curves were performed. The cell density of the cultures was measured every day using the Z2 Coulter Counter Analyzer (Beckman Coulter). After every 24 h procyclic cells were diluted to 2 x 10^6 cells mL^{-1}, whereas the bloodstream form was diluted to 2 x 10^5 cells mL^{-1}.

3.3. Selection of clones via Western Blotting

3.3.1. Sample preparation

After antibiotic selection, cell clones were chosen according to the extent of the expressed protein tag and the efficiency of the RNAi, which was visualized using western blotting. In case of RNAi-cell lines, clones were split into duplicates for cultivation in presence and absence of the RNAi-inducer doxycycline (1 µg mL^{-1}). Induced and non-induced cultures were simultaneously collected after 72 h of the first addition of doxycycline.

5 x 10^7 bloodstream cells were centrifuged at 12 °C for 10 min at 1,300x g with all supernatant discarded. The cell pellet was resuspended in 1 mL 1x phosphate-buffered saline (PBS) (137 mM NaCl, 2.7 mM KCl, 10 mM Na_2HPO_4, 1.8 mM KH_2PO_4, at a pH of 7.4) and transferred to a 1.5 mL Eppendorf tube. The tubes were subsequently spun at 12 °C for 10 minutes at

1,300x g and the supernatant was discarded. The washing procedure was repeated one more time using fresh 1x PBS. Thereafter, the cell pellet was resuspended in 32.5 µL PBS and 12.5 µL 4x lithium dodecyl sulfate (LDS) loading buffer (ThermoScientific). The sample was heated at 100 °C for 5 min and afterwards immediately placed at 4 °C, where it was kept overnight or for several days. Before being run on PAGE-gels, the lysate was sonicated at 35-40% power for 5 s, followed by the addition of 5 µL 10x sample reducing agent (ThermoScientific) to finally yield 1 x 10^6 cells μL^{-1}.

3.3.2. SDS PAGE gel electrophoresis

Once sample preparation was carried out, Bolt™ 4-12% Bis-Tris Plus (SDS) gel (ThermoScientific) was covered with 250 mL of running buffer consisting of 12.5 mL 20x Bolt™ MOPS SDS Running buffer (ThermoScientific) and 237.5 mL MiliQ H_2O. Prior to sample loading, the wells of the gel were gently cleaned with MOPS buffer with a syringe. Next, 5 x 10^6 cells per well were loaded and then ran at 160 V until the bromophenol blue dye approached the bottom of the gel.

3.3.3. Western Blotting

Before the transfer, the polyvinylidene difluoride (PVDF) blotting membrane (GE Healthcare Life Science) was submerged for 10 min in methanol to activate it. Subsequently, the membrane, as well as the gel and the filter papers, were soaked for 10 min in pre-cooled transfer buffer (25 mM Tris, 190 mM glycine, 20% methanol, pH 8.3) and placed into the transfer apparatus (Bio-Rad). The transfer apparatus was equipped with an ice pack and filled with pre-cooled transfer buffer to prevent overheating while running at 130 V for approximately 2 ½ h. After transfer, the membrane was blocked at 4 °C overnight using 1x PBS-T (1x PBS with 0.5% (v/v) Tween20) containing 4% (w/v) powdered milk. Thereafter, the membrane was incubated at room temperature for 2 h with a primary antibody (Table V), which was diluted in 1x PBS-T containing 4% (w/v) powdered milk, at constant rotation. Then, the membrane was washed three times for 5, 10 and 20 minutes with fresh 1x PBS-T. Next, the secondary antibody was diluted in 1x PBS-T containing 4% (w/v) powered milk (1:1000) and probed on the membrane at room temperature for 1 h at constant rotation. After that, the membrane was washed three times for 5, 10 and 20 minutes with fresh 1x PBS-T.

For the visualization of the probed proteins, the Clarity Max Western Peroxide Reagent and Clarity Max Western Luminol/Enhancer Reagent (1:1) (Bio-Rad) were combined and spread

out on the membrane. The chemiluminescent detection was carried out with ChemiDoc XRS+ using the corresponding Image Lab software (Bio-Rad).

Table V: Antibodies used to detect epitopes/proteins.

Primary Antibody	Secondary Antibody	Dilution Primary	Dilution Secondary
Anti-HA (ThermoScientific)	Anti-mouse	1:2000	1:1000
Anti-V5 (ThermoScientific)	Anti-mouse	1:2000	1:1000
Anti-α-Tubulin (ThermoScientific)	Anti-mouse	1:3500	1:1000

3.4. Protein analysis via Western blotting

3.4.1. NP-40 fractionation

For separation and investigation of cytoskeletal and the cytoplasmic fractions of *T. brucei*, we applied the procedure described by Concepción-Acevedo *et al.* (2012). 5 x 10^7 bloodstream form cells were collected and centrifuged at 4 °C for 10 min at 1,300x g with all supernatant discarded, followed by 2 washes with ice-cold 1x PBS buffer at 4 °C for 10 min at 1,300x g. Next, the cell pellet was resuspended in 100 µL of NP-40 buffer, comprising of 10 mM Tris-HCl, 1 mM $MgCl_2$ and 0.25% (v/v) Igepal, pH 7.4. The suspension was centrifuged at 13,000x g for 5 min at 4 °C. The supernatant was transferred to a fresh Eppendorf tube, whereas the pellet was washed 2 times with 1 mL of NP-40 buffer. Eventually, the pellet, corresponding to the non-soluble cytoskeleton, was resuspended in 100 µL of NP-40 buffer. Finally, 10 µL of each fraction was mixed with 5 µL of 4x lithium dodecyl sulfate (LDS) loading buffer (ThermoScientific), heated at 100 °C for 5 min and placed overnight at 4 °C. Before being loaded on PAGE-gels, 2 µL 10x sample reducing agent (ThermoScientific) and 3 µL MiliQ H_2O were added to yield 5 x 10^6 cells per 20 µL sample volume.

The preparation of the SDS PAGE gel electrophoresis was done according to 3.3.2. and the western blotting according to 3.3.3.

3.4.2. Investigation of tyrosine phosphorylation via Western blotting

3.4.2.1. Whole cell lysate

The experimental procedure we used is based on Nett *et al.* (2009), where the method was slightly modified. 1 x 10^8 of induced and non-induced procylic cells were collected and centrifuged at 4 °C for 10 min at 1,300x g discarding the supernatant. Then, the cells were

washed in ice-cold 1x PBS buffer and centrifuged at 4 °C for 10 min at 1,300x g. The washing procedure was repeated twice, each time with fresh 1x PBS. Afterwards, the cells were lysed with 100 µL ice-cold RIPA lysis buffer containing 10 mM Tris-HCl at pH 7.5, 1 mM sodium-β-glycerophosphate, 1mM sodium-pyrophosphate, 1mM sodium fluoride, 5 mM EDTA, 0.5% (v/v) NP-40, 0.2% (w/v) sodium-deoxycholate, 0.2% (w/v) sodium dodecyl sulfate (SDS), EDTA-free protease inhibitor tablet (Roche) and 100 µM activated sodium-orthovanadate. The lysate was sonicated three times for 5 s at 35-40% power at 4 °C and centrifuged at 16,100x g for 20 min at 4 °C. The resulting supernatant was collected, and its protein concentration measured using Pierce™ 660nm Protein Assay Reagent (ThermoScientific). Finally, 10 µg of proteins were mixed with the appropriate volume of 4x lithium dodecyl sulfate (LDS) loading buffer (ThermoScientific), heated at 100 °C for 5 min and placed overnight at 4 °C.

Induced and non-induced procyclic cells were collected and harvested simultaneously after 6 days of the first addition of 1 µg mL^{-1} doxycycline.

3.4.2.2. MME fractionation

3 x 10^7 procyclic or bloodstream cells were collected, centrifuged at 4 °C for 10 min at 1,300x g with all supernatant discarded and washed by repeating centrifugation 2 times with ice-cold 1x PBS buffer each time at 4 °C for 10 min at 1,300x g (Nett *et al.*, 2009). In order to investigate the distribution of TbPH1, TbKIFx and the phosphotyrosine -containing proteins between the cytosolic and cytoskeletal fractions, the cells were lysed in 100 µL ice-cold MME buffer (10 mM MOPS at pH 6.9, 1 mM EGTA, 1 mM $MgSO_4$) containing EDTA-free protease inhibitor tablet (Roche), 0.2% (v/v) Triton X-100. MME was supplemented with phosphatase inhibitor cocktail of 1 mM sodium-β-glycerophosphate, 1 mM sodium-pyrophosphate, 1 mM sodium fluoride, and 100 µM activated sodium-orthovanadate. For efficient lysis, the cells were incubated on ice for 30 min and then centrifuged at 13,000x g for 2 min at 4 °C. The resulting supernatant was collected in a new Eppendorf tube, and the pellet washed 3 times, each time using 1 mL MME buffer the previous mentioned phosphatase inhibitor cocktail. The insoluble cytoskeletal fraction was solubilized in 100 µL RIPA lysis buffer, which composition is described in 3.4.2.1. After that, the protein concentration in the different fractions was measured using the Pierce™ 660nm Protein Assay Reagent (ThermoScientific). Eventually, 10 µg of proteins of each fraction was mixed with the appropriate volume of 4x

lithium dodecyl sulfate (LDS) loading buffer (ThermoScientific), heated at 100 °C for 5 min and placed overnight at 4 °C.

3.4.2.3. SDS PAGE gel electrophoresis

For proper protein separation, a 10% SDS PAGE gel was prepared. Thus, 4 mL of H_2O, 3.3 mL of 30% Acrylamide mix (w/v), 2.5 mL of 1.5 M Tris (pH 8.8), 0.1 mL of 10% SDS (w/v), 0.1 mL of 10% Ammonium persulfate (APS) (w/v) and 4 µL Tetramethylethylenediamine (TEMED) were mixed, covered with MiliQ H_2O and left to polymerize for approximately 1 h. In the meantime, the stacking gel was prepared mixing 2.1 mL MiliQ H_2O, 500 µL of 30% Acrylamide mix (w/v), 380 µL of 1.0 M Tris (pH 6.8), 30 µL of 10% SDS (w/v), 30 µL of 10 % of APS (w/v) and 3 µL TEMED. Immediately after the stacking gel preparation, the MiliQ H_2O layer, covering the separation gel, was quickly removed and the stacking gel mixture was instantly poured over the separation gel. Upon complete polymerization of the stacking gel, the SDS PAGE gel was covered with 250 mL of running buffer consisting of 25 mM Tris, 192 mM glycine and 0.1% (w/v) SDS. Then, the wells of the gel were gently cleaned with running buffer via a syringe.

Prior to sample loading, the sample was briefly heated at 100 °C until the SDS dissolves. Thereafter, an appropriate volume of 10x sample reducing agent (ThermoScientific) was added to each sample. Subsequently, the samples were loaded and ran at 100 V until the bromophenol blue dye approached the bottom of the gel.

3.4.2.4. Western Blotting

The preparation of the PVDF blotting membrane (GE Healthcare Life Science) and electrophoresed gel, as well as the assembly of the transfer apparatus and transfer were done in the same way as in section 3.3.3.

After the transfer, the membrane was blocked at room temperature for 1 h in 1x TBS-T (1x Tris Buffered Saline (TBS) with 0.2% (v/v) Triton X-100) containing 4% (w/v) Bovine Serum Albumin (BSA) (Sigma-Aldrich). Next, the membrane was incubated at room temperature for 1 h with a primary antibody (Table VI), which was diluted in 1x TBS-T containing 4% (w/v) BSA, at constant rotation. Thereafter, the membrane was washed three times for 5, 10 and 20 minutes with fresh 1x TBS-T. This was followed by incubation at room temperature for 1 h at constant rotation with the secondary antibody diluted (1:1000) in 1x TBS-T containing 4% (w/v) BSA. Then, washing steps of 5, 10 and 25 min were performed using each time fresh 1x TBS-T. Visualization of immunodecorated proteins was done as described in section 3.3.3.

Table VI: Antibodies used to detect epitopes/ proteins of interest.

Primary Antibody	Secondary Antibody	Dilution Primary	Dilution Secondary
Anti-Phosphotyrosine, clone 4G10 (Merck)	Anti-mouse	1:5000	1:1000
Anti-HA (ThermoScientific)	Anti-mouse	1:2000	1:1000
Anti-V5 (ThermoScientific)	Anti-mouse	1:2000	1:1000
Anti-α-Tubulin (ThermoScientific)	Anti-mouse	1:3500	1:1000

3.4.2.5. Negative control for Anti-Phosphotyrosine

A replicate blot was processed to serve as negative control for the anti-phosphotyrosine antibody (Nett *et al.*, 2009). The blot was incubated in alkaline phosphatase buffer (50 mM Tris-HCl at pH 8.5, 5 mM $MgCl_2$) containing 15 units of shrimp alkaline phosphatase (Affymetrix) at 30 °C overnight. Thereafter, the control blot was washed 3x for 5 min with TBS-T and probed with anti-phosphotyrosine antibody. The western blot was performed in the same way as described in 3.4.2.4.

3.4.2.6. Coomassie blue staining

The gel was fixed in a mixture of 50% methanol and 10% glacial acetic acid for approximately 1 h at constant agitation. Thereafter, the gel was gently washed with MiliQ H_2O and stained for 20 min in a solution containing 0.1% Coomassie Brilliant Blue R-250, 50% methanol and 10% glacial acetic acid. Again, MiliQ H_2O was used to rinse the gel and to wash away the excess of the staining solution. Finally, the gel was destained by incubation in 40% methanol and 10% glacial acetic acid for several hours with several changes of the solution. A paper towel was submerged with the gel to accelerate the destaining process.

3.5. Immunofluorescence Assay

3.5.1. Sample preparation

We performed IFAs on *T. brucei* to determine the localization of TbKIFx and TbPH1. Therefore, 1 mL of mid-log procyclic cells (approximately 1x 10^7 cells mL^{-1}) and 10 mL of mid -log bloodstream cells (approximately 1x 10^6 cells mL^{-1}) were collected and centrifuged at room temperature for 10 min at 1,300x g to discard the media. Next, cells were shortly washed with 1x PBS and spun at room temperature for 5 min at 1,300x g with all supernatant removed.

3.5.2. Whole cell preparation

After the washing step with 1x PBS, the cells were resuspended in 1 mL of 4% (w/v) paraformaldehyde (PFA) in 1x PBS and 1.25 mM NaOH, spread over the whole Superfrost plus® slide (ThermoScientific) and left to settle for 10 min. Subsequently, cells were permeabilized for 20 min with 0.2 % (v/v) Triton X-100 in 1x PBS.

3.5.3. NP-40 fractionation

The experimental procedure is more or less identical to the one proposed by Concepción-Acevedo *et al.* (2012). The washed cell pellet was resuspended in 250 µL of NP-40 buffer (10 mM Tris-HCl, 1 mM $MgCl_2$ and 0.25% (v/v) Igepal, at pH of 7.4), spread over the whole Superfrost plus® slide (ThermoScientific) and incubated on ice for 5 min. Afterwards, the cells were shortly washed in 1x PBS and fixed with 4% (w/v) PFA in 1x PBS and 1.25 mM NaOH.

3.5.4. MME fractionation

The procedure to extract the cytoskeleton via MME buffer is essentially the same as that used by Nett *et al.* (2009). The cell pellet was resuspended in 300 µL 1x PBS and spread over the whole Superfrost plus® slide (ThermoScientific). The cells were settled onto the slide for 15 min and thereafter incubated on ice for 10 min with 500 µL MME buffer (10 mM MOPS at pH 6.9, 1 mM EGTA, 1 mM $MgSO_4$), where 3 changes of the buffer were performed. Next, cells were washed with 1x PBS and fixed for 10 min in 4 % (w/v) PFA in 1x PBS and 1.25 mM NaOH.

3.5.5. MME Flagellum isolation

The flagellum isolation was prepared according to the procedure used by Nett *et al.* (2009). Thus, the cell pellet was resuspended in 300 µL 1x PBS, spread over the whole Superfrost plus® slide (ThermoScientific) and settled for 15 min. The isolation of the flagellar complex was achieved by incubating the cells on ice for 15 min with MME buffer containing 1 M NaCl, where the buffer was changed 3 times. Afterwards, the cells were washed with 1x PBS, followed by their fixation for 10 min in 4 % (w/v) PFA in 1x PBS and 1.25 mM NaOH.

3.5.6. PEME fractionation

1 mL of mid-log procyclic cells (approximately 1x 10^7) were collected and centrifuged at room temperature for 5 min at 800x g with all supernatant discarded. Thereafter, the cell pellet was resuspended in 1 mL 1x PBS and centrifuged once again at room temperature for 5 min at 800x g to remove the PBS. Next, cells were resuspended in 1 mL of 1x PBS (1x 10^7 cells mL^{-1}), where 4 drops, each of 80 µL, were distributed on the Superfrost plus® slide (ThermoScientific). The drops were left on the slide for several minutes to ensure a proper settling of the cells. Subsequently, the liquid was removed using a pipette, and 60 µL of PEME (100 mM piperazine-N,N′-bis(2-ethanesulfonic acid) (PIPES) at pH 6.9, 1 mM $MgSO_4$, 2 mM EGTA, 0.1 mM EDTA) containing 0.5% (v/v) NP-40 (Igepal) was placed for 10 s on the cell spots, while carefully rocking the slide inside the palm of my hand. The PEME was then quickly removed, and the cells were eventually fixed for 10 min with 4 % (w/v) PFA in 1x PBS and 1.25 mM NaOH. To decrease potential PFA-induced fluorescent background, slides were treated for 10 min with 30 mM glycine in 1x PBS at pH 7.5.

3.5.7. Probing with antibodies

Before blocking, the slides were washed in 1x PBS regardless of used sample preparation protocol. The cells were blocked at room temperature for 1 h using 2% (w/v) fish gelatine in 1x PBS containing 0.2% (v/v) Triton X-100. After that, the slides were washed once with 1x PBS to remove the blocking solution. Then, the slide was incubated at room temperature for 50 min with primary antibody (dilutions given in Table VII), which was diluted in 1x PBS containing 2% (w/v) fish gelatine and 0.2% (v/v) Triton X-100. Thereafter, the slides were washed 3 times with 1x PBS, followed by the incubation with the appropriate secondary antibody (Table VII) at room temperature for 40 min diluted in 1x PBS containing 2% (w/v) fish gelatine and 0.2% (v/v) Triton X-100. During incubation with the secondary antibody, light was obstructed from the slides to prevent any bleaching of the fluorescent signal of the

secondary antibody. Next, 3 washing steps were performed using 1x PBS. Finally, a drop of ProLong™ Gold antifade reagent with DAPI (ThermoScientific) and a cover slips were placed on the slides, where the edges of the cover glasses were sealed with regular nail polish after about 12 h. The slides were stored at 4 °C in the dark overnight or for several days until the fluorescent signal was visualized using the fluorescent microscope Axioplane 2 (Zeiss).

Table VII: Antibodies used for indirect immunofluorescence assays.

Primary Antibody	Secondary Antibody	Dilution Primary	Dilution Secondary
Anti-HA, monoclonal, IgG (ThermoScientific)	Anti-mouse (ThermoScientific)	1:1000	1:1000
Anti-V5, polyclonal, IgG (ThermoScientific)	Anti-rabbit (ThermoScientific)	1:1000	1:1000
Anti-V5, monoclonal, IgG (ThermoScientific)	Anti-mouse (ThermoScientific)	1:1000	1:1000
Anti-Phosphotyrosine, clone 4G10, monoclonal, IgG (Merck)	Anti-mouse (ThermoScientific)	1:1000	1:1000
Mature basal body YL 1/2, monoclonal, IgG (Kilmartin, 1982)	Anti-rat (ThermoScientific)	1:50	1:1000
FAZ filaments L3B2, monoclonal, IgG (Kohl *et al.*, 1999)	Anti-mouse (ThermoScientific)	1:3	1:1000
PFR L8C4, monoclonal, IgG (Kohl *et al.*, 1999)	Anti-mouse (ThermoScientific)	1:100	1:1000
MtQ 1B41, monoclonal, IgM (Gallo *et al.*, 1988)	Anti-mouse, IgM (ThermoScientific)	1:1000	1:1000

3.6. SEM preparation

The localization of TbKIFx was examined by scanning electron microscopy (SEM). The bloodstream cells were prepared in the same way as in 3.5.1. For cytoskeleton extraction, the procedure described in 3.5.4. was applied, followed by blocking and probing with antibodies according to 3.5.7. In this case, the secondary antibody was conjugated with 5 nm gold (Table VIII). Upon incubation with the secondary antibody, the Superfrost plus® slides (ThermoScientific) were submerged in 1x PBS and kept at 4°C overnight.

All further steps as well as the visualization by the electron microscope were carried out by RNDr. Marie Vancová, Ph.D. (Institute of Parasitology, Biology Centre, Czech Academy of Sciences). After the incubation at 4°C overnight in 1x PBS, the cytoskeletons were once again fixed in 2.5% glutaraldehyde in 0.1 M PB (phosphate buffer without salt) for 15 min.

Thereafter the slide was washed 3x times with 0.1 M PB, postfixed in 1% OsO_4 for 15 min and dehydrated in a series of 30, 50, 70, 90 and 100% acetone; each incubation was for 3-5 min. Next, the slides were dried using the critical-point drying method (Bray *et al*., 1993) using the critical point dryer CPD 2 (Pelco™) and then coated with carbon. Finally, the cytoskeletons were observed using JEOL 7401 F detecting backscattered electrons with an applied voltage of 4 kV.

Table VIII: Antibodies used for SEM preparation

Primary Antibody	Secondary Antibody	Dilution Primary	Dilution Secondary
Anti-V5, polyclonal, IgG (ThermoScientific)	Anti-rabbit protein A conjugated with 5 nm gold (Cell Biology UMC Utrecht)	1:1000	1:50

4. Results

4.1. Construct verification

Constructs for *in situ* tagging of the proteins of interest were generated by PCR amplification and subsequently verified by gel electrophoresis (Figure 8).

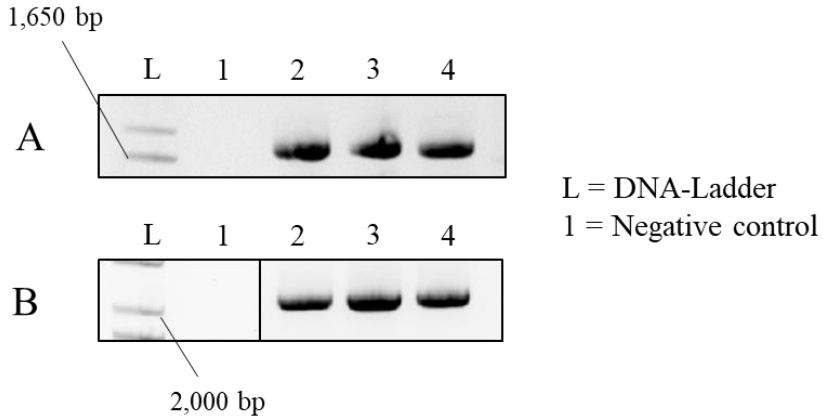

Figure 8: Gel electrophoresis verifying the PCR amplification of (A) the TbPH1-HA construct and (B) the TbKIFx-V5 construct for transfection, where the lanes (2), (3) and (4) were loaded with the respective PCR-products. Lanes (1) contained the negative control. (L) stands for DNA-Ladder.

The already generated pTrypSon RNAi-constructs (Kaltenbrunner, 2017) were linearized using high fidelity NotI and verified by gel electrophoresis (Figure 9).

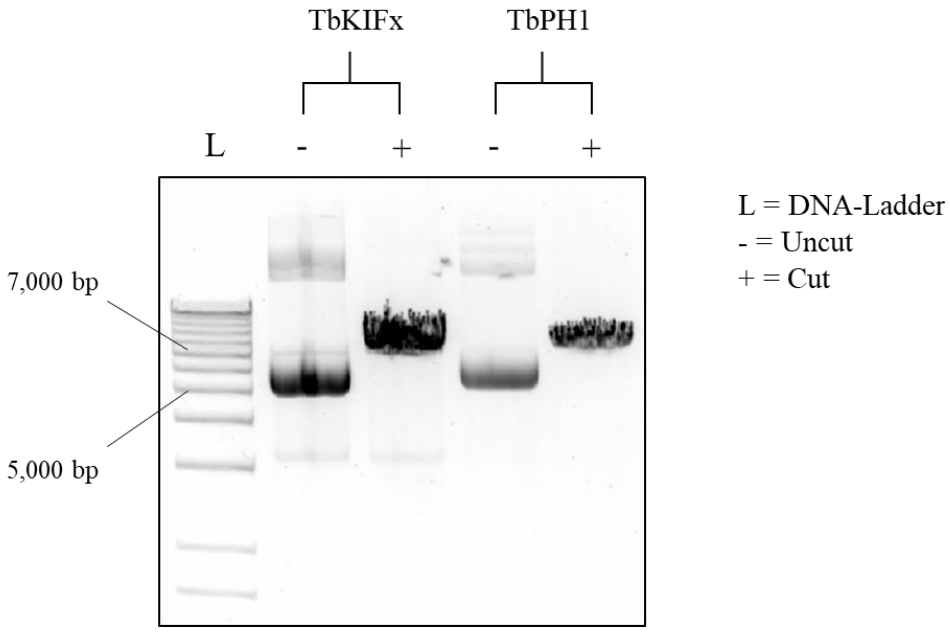

Figure 9: Verification of linearization of TbKIFx RNAi-constructs and TbPH1 RNAi-construct by gel electrophoresis. (-) represents the uncut plasmid and (+) the plasmid cut with NotI. (L) stands for DNA-Ladder. The verified linearized constructs were used for transfection.

4.2. Cell line generation

Upon transfecting SmOx B4 bloodstream cells with the TbPH1-HA construct, clones that survived antibiotic treatment (Table I) were further selected based on the expression intensity of the protein tag using western blot analysis. The membrane was probed with anti-HA antibody to be able to detect TbPH1-HA. Based on the western blot results, clone nr. 2 (Figure 10A, asterisk) was chosen and further transfected with the TbKIFx-V5 construct. Once again, several survivors were selected for western blot examinations using anti-V5 antibody to visualize TbKIFx-V5. In this case, clone nr. 4 (Figure 10B, asterisk) exhibited the highest expression of the protein tag V5 and was used for further experiments.

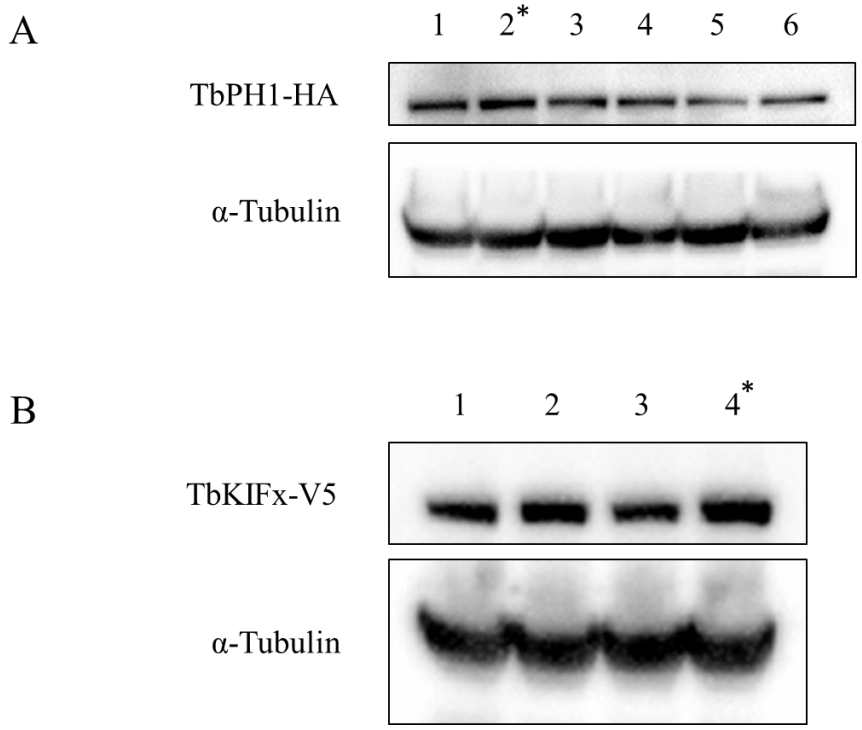

Figure 10: The extent of expression of tagged proteins were evaluated based on western blot analysis. The protein TbPH1 was HA-tagged (A), whereas TbKIFx was V5-tagged (B). According to the extent of the tagged-protein expression, clone 2 (A, asterisk) and clone 4 (B, asterisk) were chosen for further experiments. Immunodecorated α-Tubulin serves as a loading control.

To investigate the effect of depleting either TbPH1 or TbKIFx in SmOx B4, the respective RNAi-cell lines were generated expressing both TbPH1-HA and TbKIFx-V5. After the transfections and the antibiotic selection, RNAi efficiencies were tested. Therefore, clones were split into two cultures, one culture containing doxycycline to examine RNAi efficiency, and one control culture without doxycycline (Figure 11).

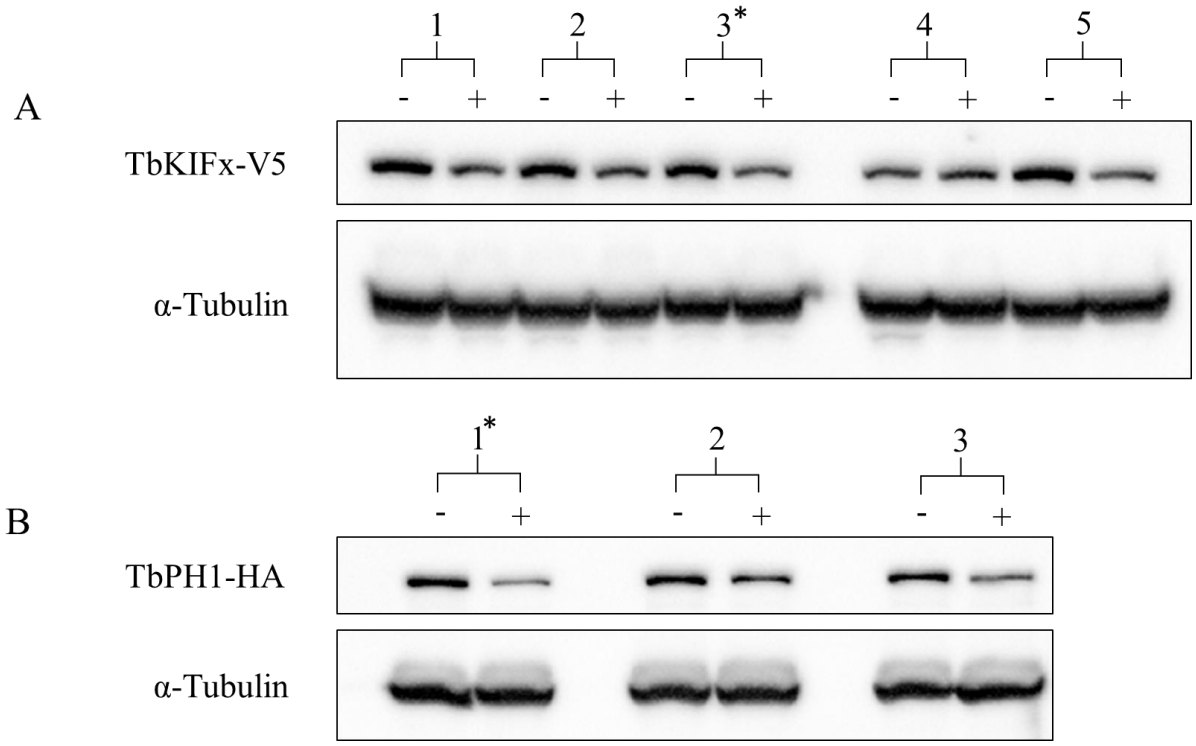

Figure 11: RNAi efficiency for (A) TbKIFx and (B) TbPH1 knockdown cell lines were evaluated by western blotting using anti-V5 antibody for TbKIFx-V5 RNAi-knockdowns and anti-HA antibody for TbPH1-HA-knockdowns (Table VI). The respective clones were split into non-RNAi induced (-) (control) and RNAi induced (+) cultures for analysing the efficiency of the depletion. Cells were induced for 72 h before harvesting. Clone 3 (A, asterisk) and clone 1 (B, asterisk) were selected due to the best downregulation of the respectively targeted protein compared to the control. Immunodecorated α-tubulin serves as a loading control.

Western blot analysis revealed low RNAi efficiency in both cell lines (Figure 11A and 11B). Therefore, we decided to discontinue working with the generated knockdown cells of TbKIFx and TbPH1. Nevertheless, clone 3 of the TbKIFx-RNAi cell line (Figure 11A, nr. 3) and clone 1 of TbPH1-knockdown cell line (Figure 11B) were chosen and stored in liquid nitrogen.

4.3. Association of TbKIFx and TbPH1 with cytoskeletal structures verified by western blotting

In order to verify the association of the kinesin TbKIFx and the kinesin-like TbPH1 with the cytoskeleton structure of long slender bloodstream form *T. brucei*, the cytoskeletal and cytoplasmic fractions of SmOx B4 expressing TbKIFx-V5 and TbPH1-HA (see Results 4.2) were separated using NP-40 buffer (see Materials and Methods 3.4.1.) and analysed by immunoblotting.

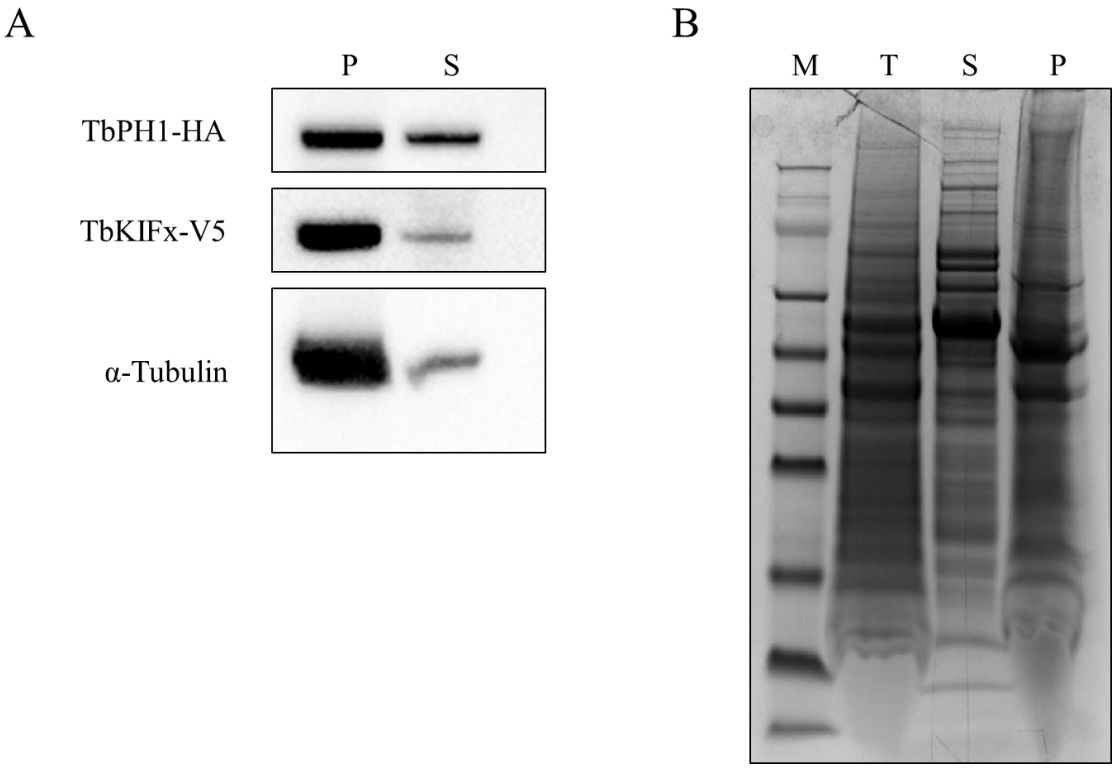

Figure 12: (A) Western blot analysis indicates the association of TbKIFx/TbPH1 with the cytoskeleton (P), where the kinesin is also to a slight extent present in the cytoplasmic fraction (S). However, TbPH1 occurs in both fractions, (P) and (S), but is more abundant in the cytoskeleton extraction. Immunodecorated α-tubulin serves as a cytoskeleton marker. (B) Coomassie blue staining served as loading control, where (T) represents the total cell lysate, (S) the cytoplasmic fraction, (P) the cytoskeletal fraction and (M) the prestained protein ladder.

Despite the slight contamination of the cytosolic fraction by α-tubulin, the NP-40 mediated cytoskeletal extraction confirmed the association of TbKIFx and of TbPH1 with the cytoskeleton part of the cell. However, TbPH1 was also found to some extent in the cytoplasmic fraction. The minor occurrence of TbKIFx in the cytosolic fraction might be due to incomplete fractionation as seen by the α-tubulin contamination in the soluble fraction (Figure 12).

4.4. Localization of TbKIFx and TbPH1 in bloodstream *Trypanosoma brucei*

In order to localize TbKIFx and TbPH1, IFA was performed on paraformaldehyde-fixed bloodstream cells expressing both TbPH1-HA and TbKIFx-V5 (Figure 13).

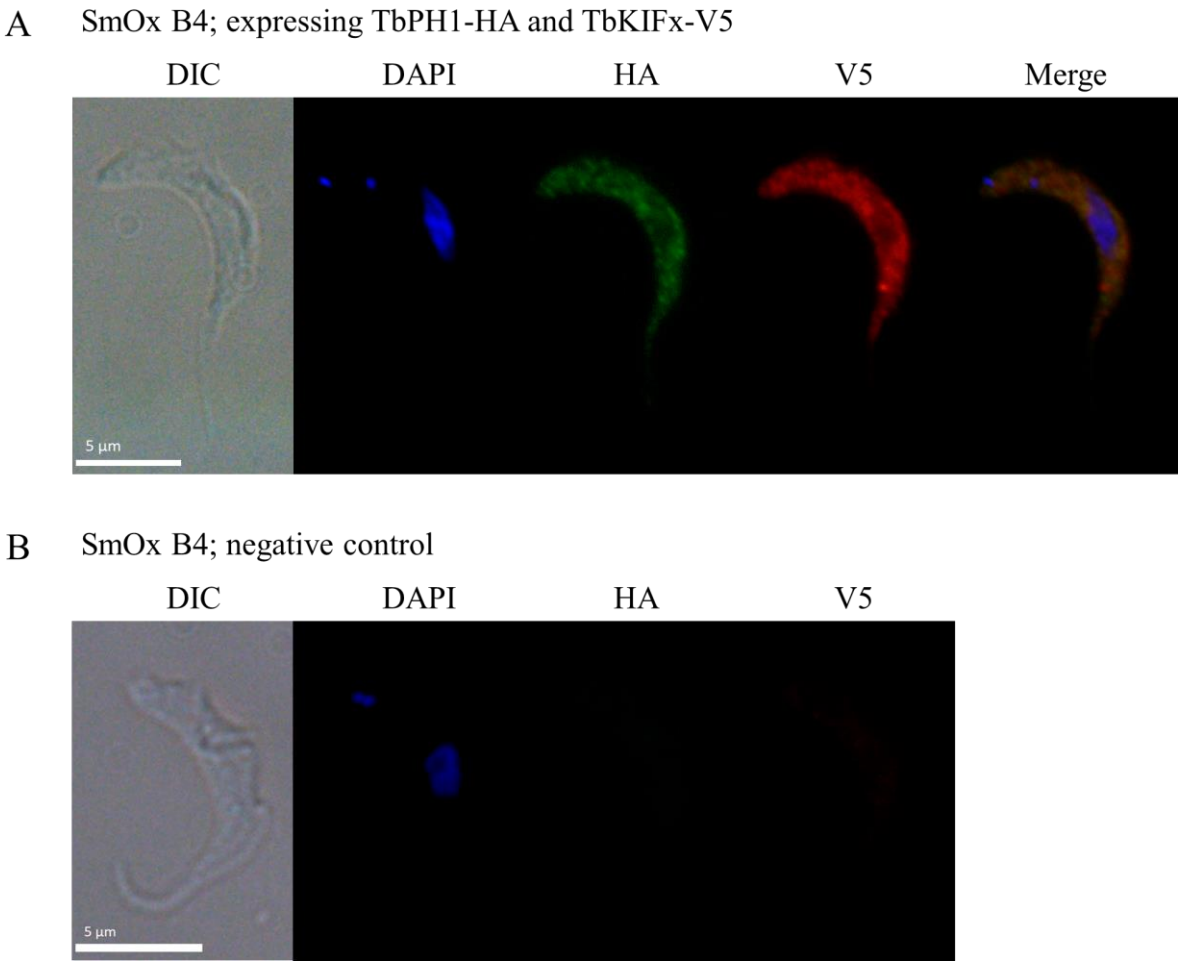

Figure 13: (A) TbKIFx-V5 (red, rabbit) and as well TbPH1-HA (green, mouse) did not show any recognizable pattern, rather seemed to be spread over the whole cell, except in the nucleus or in the kinetoplast. (B) The negative control (parental cell line SmOx B4) showed no strong signal, and thus no unspecific binding.

As observed in procyclic cells (Kaltenbrunner, 2017), both proteins were distributed throughout the cytoplasm with no recognizable pattern (Figure 13A). The lack of information led us to perform IFA on cytoskeletons extracted with NP-40 buffer to obtain a clearer and more specific signal.

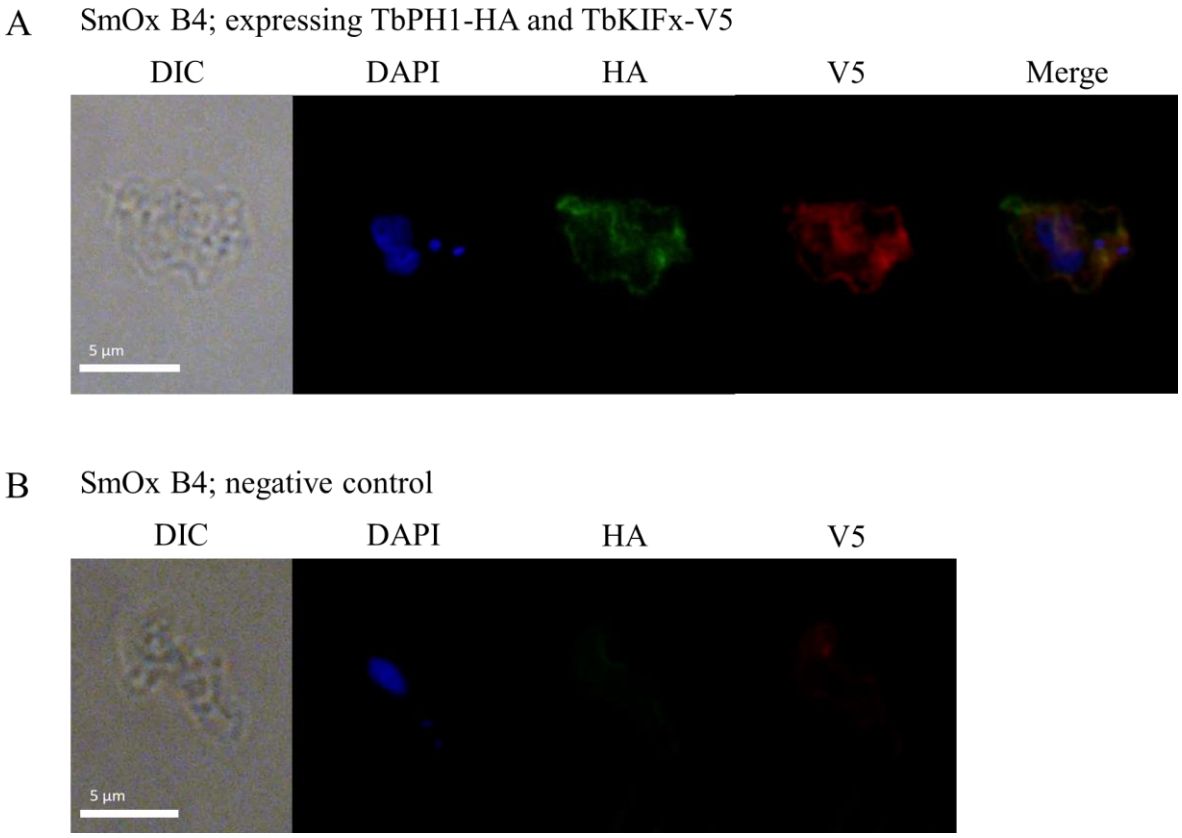

Figure 14: (A) NP-40 cytoskeleton extraction confirmed the co-localization of the proteins TbKIFx-V5 (red, rabbit) and TbPH1-HA (green, mouse), in which the signals were concentrated on specific cytoskeletal structures. (B) The parental cell line SmOx B4 (control) exhibited no strong signal, and thus negligible unspecific binding.

Indeed, TbKIFx-V5 and TbPH1-HA overlapped with a discernible pattern (Figure 14A). Moreover, certain cytoskeletal structures exhibited a higher intensity. For instance, the bright spot next to the kinetoplast might represent the BBs, whereas the other intensive labelled cytoskeleton structure might correspond to the paraflagellar rod (PFR) or the FAZ.

To determine the identity of the cytoskeletal elements containing TbKIFx and TbPH1, further IFAs were performed where TbKIFx-V5 was counterstained with either PFR, FAZ or mBB using the respective antibodies (Table VII). Due to the present co-localization of the TbKIFx-V5 and TbPH1-HA in isolated cytoskeletons (Figure 14A), TbKIFx was treated as proxy for TbPH1. Thus, we did not repeat the following IFA experiments for TbPH1-HA. To improve cytoskeleton extraction a different approach was used, mainly by changing the NP-40 Buffer to the MME buffer (described in Materials and Methods 3.5.4.).

First, the co-localization of TbKIFx-V5 and the PFR was tested. To confirm the staining of the actual PRF, the flagellum was also isolated under high salt conditions (see Materials and Methods 3.5.5.) and probed with the same antibody as the cytoskeleton extractions.

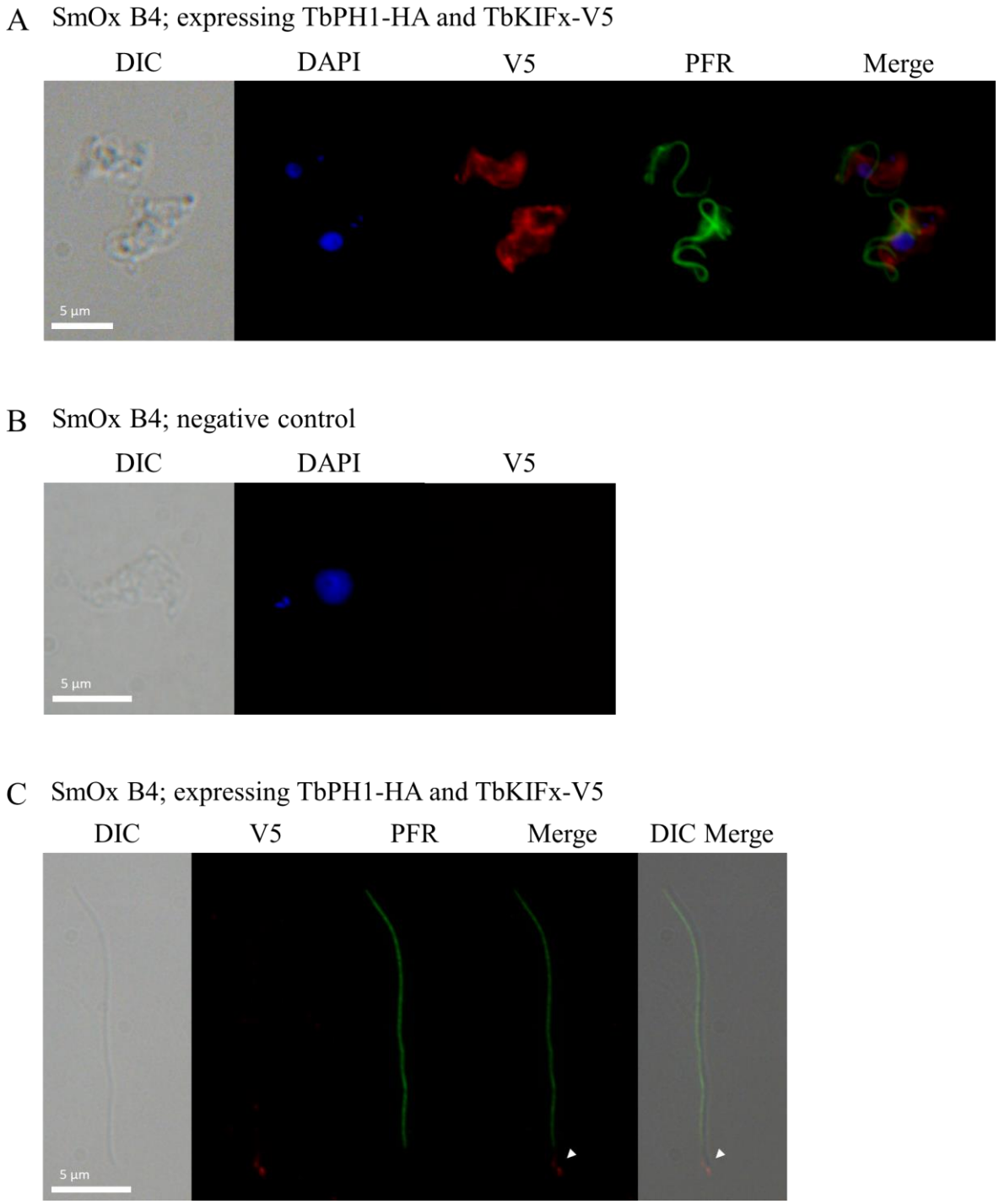

Figure 15: (A) Cytoskeleton extraction demonstrated no evidence of TbKIFx-V5 (red, rabbit) being localized on the PFR (L8C4 antibody) (green, mouse). (B) The negative control (parental cell line SmOx B4) showed no strong signal, and thus no unspecific binding. (C) The flagellum isolation demonstrated successful staining of the flagellum (L8C4 antibody) (green, mouse). Note that TbKIFx-V5 (red, rabbit) signal is located on the tip of the PFR (DIC Merge), without overlapping with the PFR signal (Merge).

TbKIFx-V5 showed a different localization than PFR (Figure 15A) in cytoskeleton extractions. Surprisingly, in flagellum isolations TbKIFx-V5 appeared to be concentrated at the base of the flagellum (Figure 15C), which might represent the BBs (Nett *et al.*, 2009).

Finally, TbKIFx was labelled in combination with either FAZ filaments or mBB on cytoskeleton extractions.

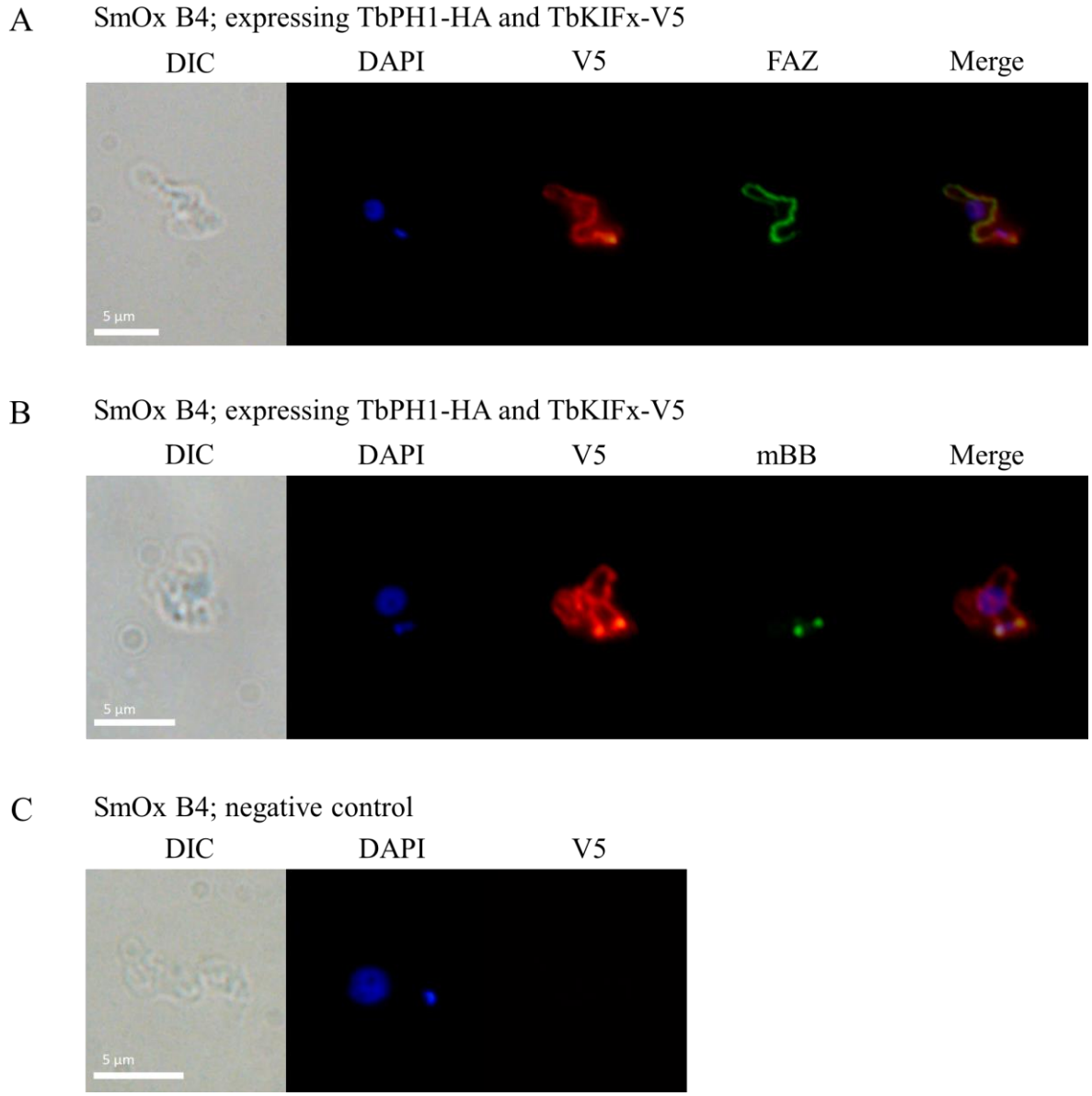

Figure 16: (A) TbKIFx-V5 (red, rabbit) co-localized with FAZ filaments (L3B2 antibody) (green, mouse). Note TbKIFx-V5 signal extends to another cytoskeletal structure, which is not part of the FAZ. This cytoskeletal element was identified as the mBB (YL 1/2 antibody) (green, rat) (B). (C) The negative control (parental cell line SmOx B4) showed no strong signal, and thus no unspecific binding.

Interestingly, both cytoskeletal structures, FAZ filaments and mBB, overlapped with the signal of TbKIFx-V5 (Figure 16), where the signal at the mBB is highly enriched. Furthermore, the signal of TbKIFx-V5 seemed to connect the mBB and the FAZ filaments. However, the FAZ filaments and basal bodies are not directly associated with each other. Only the MtQ functions as link between the two cytoskeletal compartments (Vaughan & Gull, 2015; Sunter & Gull, 2016). Hence, TbKIFx/TbPH1 dimer might interact with the MtQ and use it as a route for potential transport of its still unknown cargo.

4.5. SEM data further supports the potential interaction of TbKIFx/TbPH1 with MtQ

To elucidate the actual location of TbKIFx/TbPH1 on the cytoskeleton, we probed TbKIFx-V5 with a secondary antibody conjugated with 5 nm gold in bloodstream cytoskeleton extractions (see Materials and Methods 3.6). The visualization of the immunogold labelled TbKIFx-V5 was attained by scanning electron microscopy (SEM) using the back-scattered electrons (YAG) (Autrata, 1992).

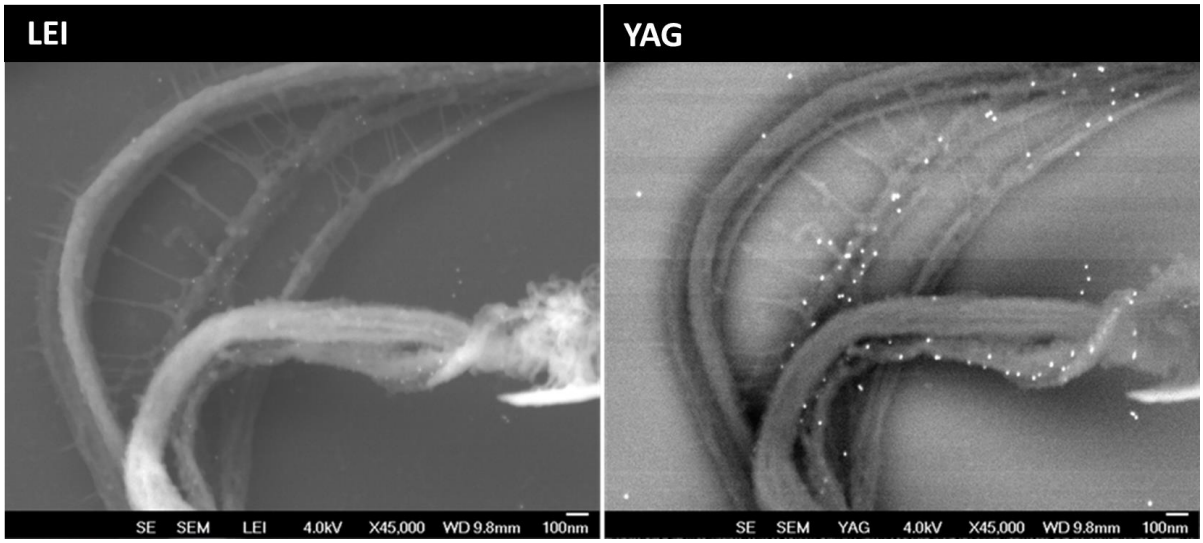

Figure 17: (Left) The topology of bloodstream *T. brucei* cytoskeleton extraction was visualized by the secondary electron detector (LEI). The image shows the flagellum, the partially attached FAZ filaments and the associated MtQ (Figure 2 & 3). (Right) Using the back-scattered electron detector (YAG), TbKIFx conjugated with 5 nm gold was detected on the supposed MtQ (Autrata, 1992). Both images were taken with the following parameters: voltage = 4.0 kV, magnification x45,000, working distance (WD) = 9.8 mm.

The SEM images (Figure 17) revealed the specific binding of TbKIFx-V5 to a structure, which appears to run along the PFR. Only MtQ and FAZ filaments are located along the PFR (Sunter & Gull, 2016). These images agree with previous results (see Results 4.4., Figure 16) and therefore strengthen the hypothesis of TbKIFx co-localizing with MtQ.

4.6. TbPH1 and TbKIFx co-localize with the MtQ and mBB in procyclic *Trypanosoma brucei*

Using the NP-40 or the MME buffer for cytoskeleton extractions in IFAs, individual cytoskeleton structures were difficult to identify. For this reason, the piperazine-N,N′-bis(2-ethanesulfonic acid) (PIPES) based PEME buffer was chosen to perform further cytoskeletal isolations (see Materials and Methods 3.5.6.). Moreover, the fragile cytoskeleton of bloodstream *T. brucei* led to the decision to switch our focus on the procyclic form, which offers a more robust cytoskeleton.

To check if TbPH1 and TbKIFx co-localize in procyclic cells, cytoskeleton extraction was performed on SmOx P9 expressing TbPH1-V5 and TbKIFx-HA (Figure 18).

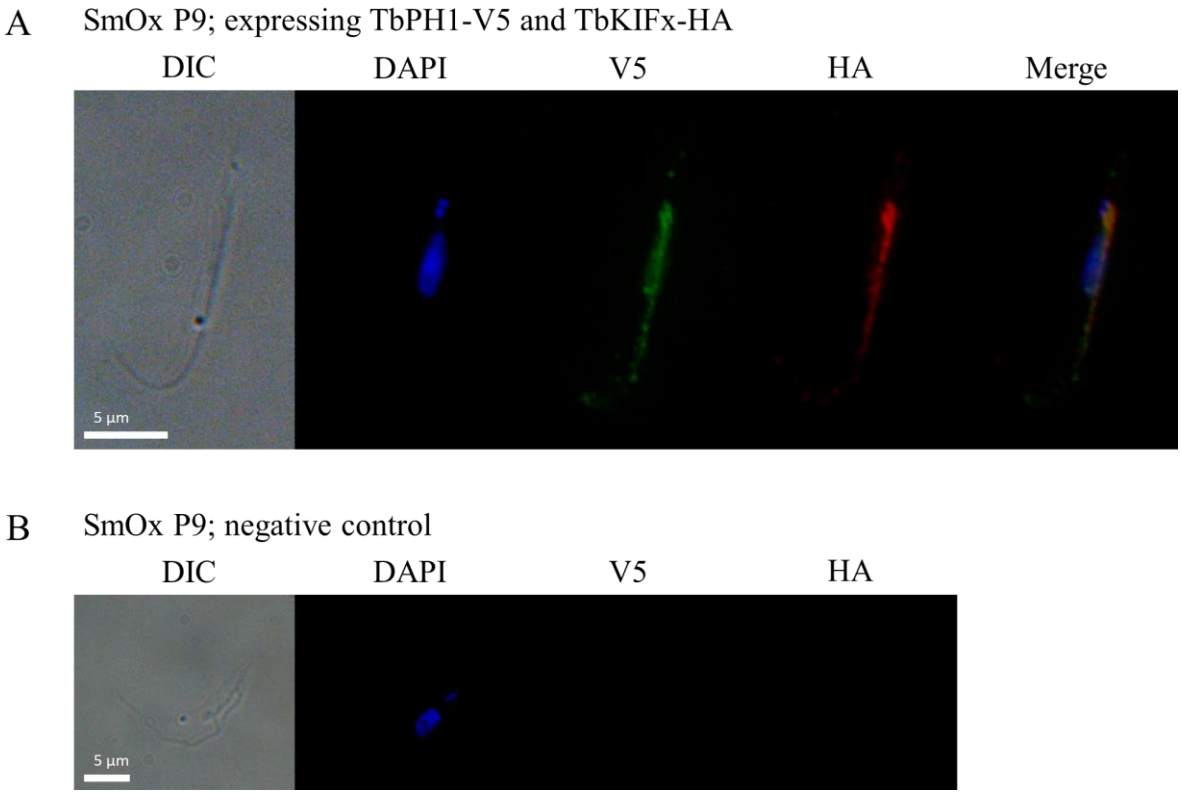

Figure 18: (A) Cytoskeleton extraction of procyclic *T. brucei* confirmed the co-localization of TbPH1-V5 (green, rabbit) and TbKIFx-HA (red, mouse), where the signal was concentrated around the kinetoplast and along the PFR. (B) The parental cell line SmOx P9 (control) exhibited no strong signal, and thus no unspecific binding.

The shape of the extracted cytoskeletons was highly improved using PEME buffer. Furthermore, the IFA analysis revealed the co-localization of TbPH1-V5 and TbKIFx-HA in procyclic cells, where the proteins were concentrated near the kinetoplast and along the FAZ. Thus, both proteins might possess the same localization as in the bloodstream form.

In order to prove our hypothesis of MtQ representing the binding-site of TbKIFx/TbPH1, further IFAs were performed labelling TbPH1 in combination with either the MtQ or the mBB, where we decided to proceed with procyclic cells and the PEME buffer-treatment due to the achieved improvement of cytoskeleton extractions (Figure 18).

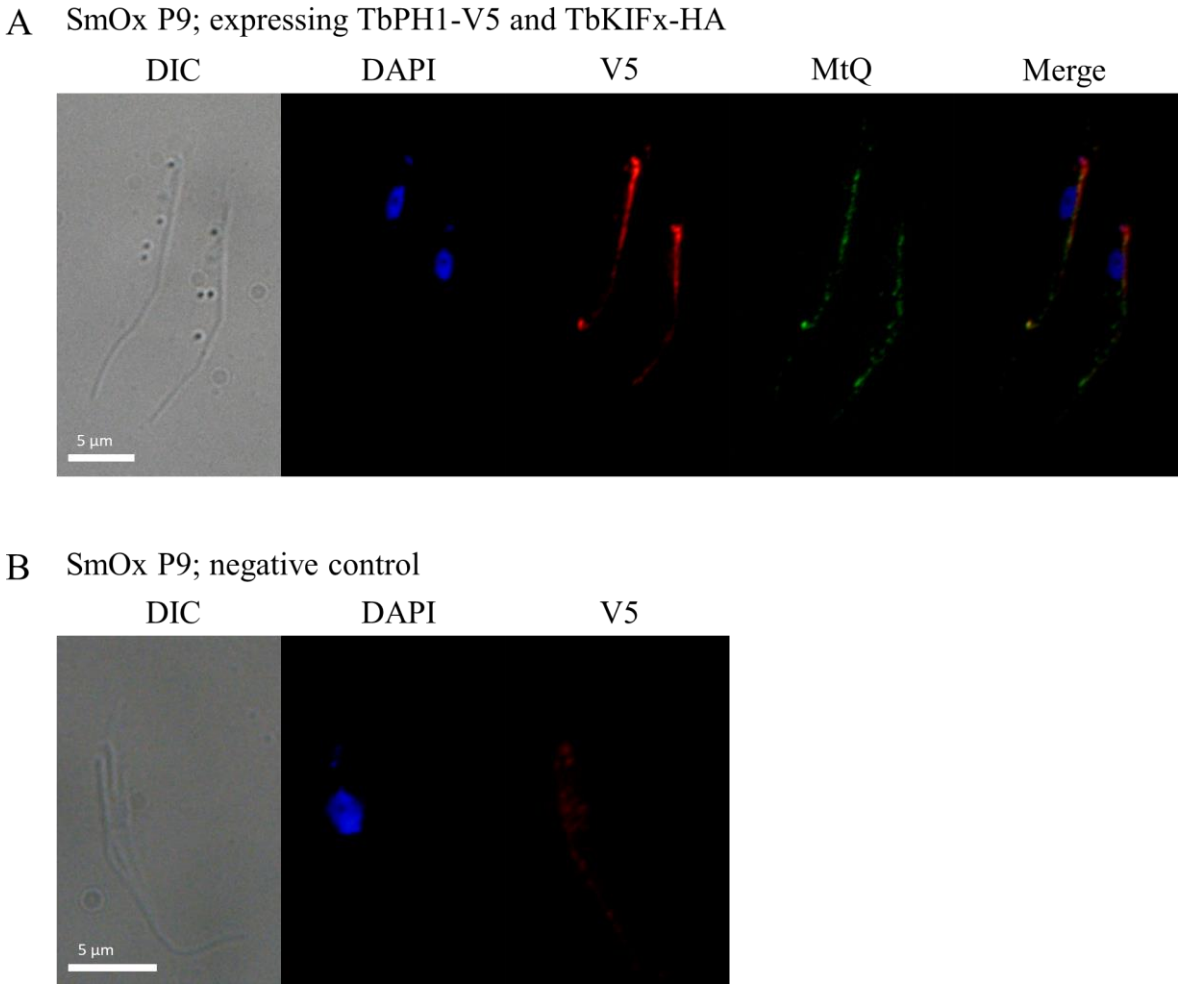

Figure 19: (A) TbPH1-V5 (red, rabbit) co-localized with the MtQ (1B41 antibody) (green, mouse) in cytoskeleton extracted from procyclic cells. (B) The parental cell line SmOx B4 (control) exhibited a slight signal, which indicated a small extent of unspecific binding to other structures.

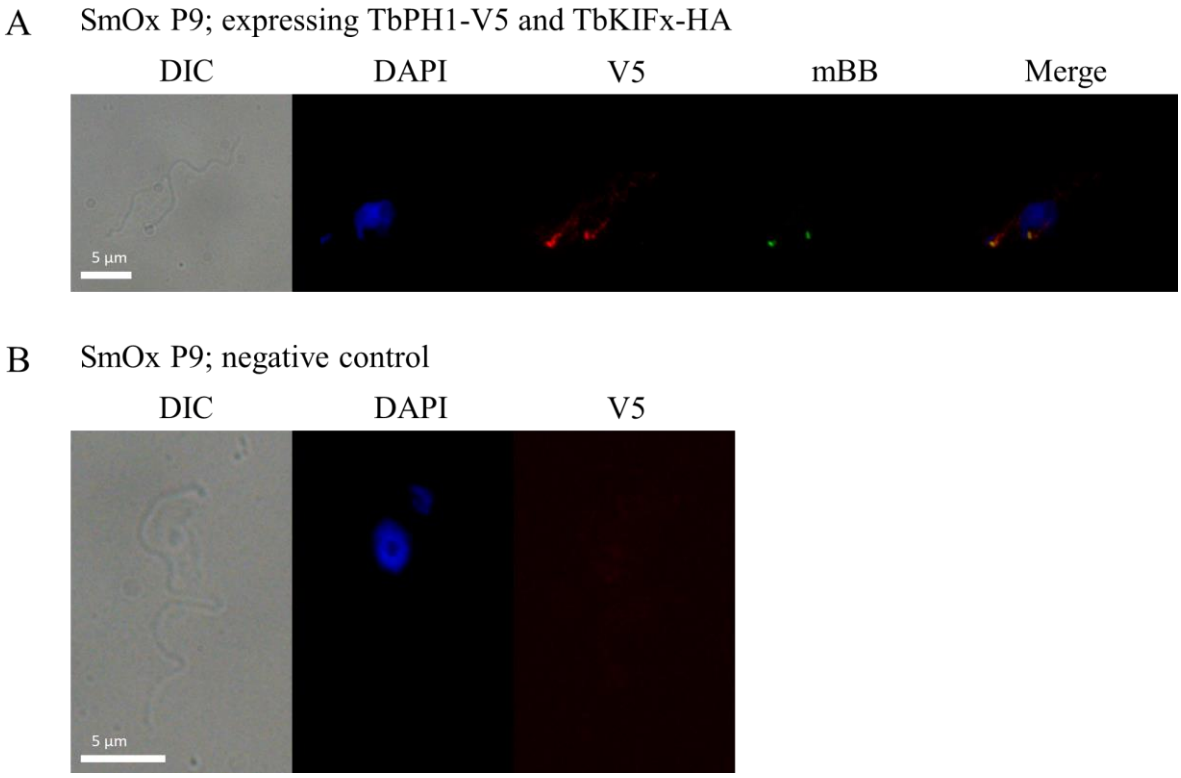

Figure 20: (A) In cytoskeletons extracted from procyclic *T. brucei*, TbPH1-V5 (red, mouse) strongly overlapped with the mBB (YL 1/2, rat). (B) The control (parental cell line SmOx B4) exhibited no strong signal, and thus no occurrence of unspecific binding.

The TbPH1-V5 signal overlapped with the labelled MtQ (Figure 19A) with an intensive TbPH1 spot near the kinetoplast co-localizing with the mBB (Figure 20A). Therefore, these IFA results further support the hypothesis that TbPH1/TbKIFx bonds the MtQ and the mBB. In addition, the findings (Figure 19 & 20) are in agreement with the previous results in the bloodstream form (Figure 16), indicating that both bloodstream and procyclic life cycle stage share the same cytoskeletal localization of TbKIFx/TbPH1.

4.7. The role of TbPH1 in the relationship with TbKIFx

Even though we were able to localize TbKIFx and TbPH1 in bloodstream cells by IFA and SEM, the function of the associated proteins remained unclear. For this reason, the investigation was focused on the PH domain of TbPH1, the only indication of a potential function. Therefore, the relation between TbPH1/TbKIFx and tyrosine-phosphorylation was analysed assuming that the PH-domain of TbPH1 interacts with tyrosine-phosphorylated proteins (p-Tyr).

In order to examine whether cytoskeleton associated tyrosine-phosphorylated proteins (Nett *et al.*, 2009) co-localize with TbKIFx, and therefore with TbPH1, we performed IFA on MME mediated cytoskeleton extracted bloodstream cells (Figure 21).

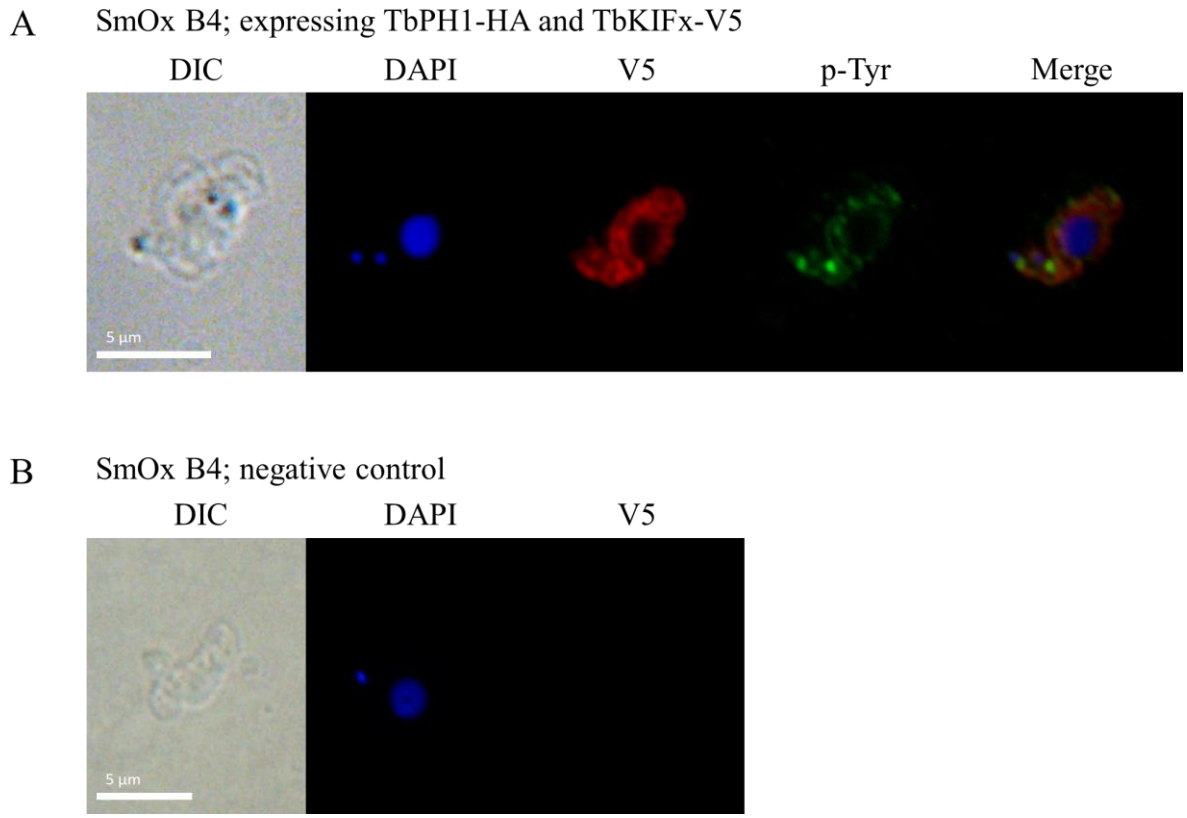

Figure 21: (A) The cytoskeleton extraction confirmed the co-localization of TbKIFx-V5 (red, rabbit) and p-Tyr proteins (green, mouse) in bloodstream *T. brucei*. (B) The negative control (parental cell line SmOx B4) showed no strong signal, hence no unspecific binding.

Remarkably, the signal of TbKIFx and tyrosine-phosphorylated proteins overlapped to a high degree (Figure 21), thus pointing to a potential interaction.

To investigate the potential interaction of TbKIFx/TbPH1 with tyrosine-phosphorylated proteins, we decided to perform western blot analysis on procyclic TbKIFx knockdowns (see Materials and Methods 3.4.2.). The RNAi-knockdown of TbKIFx appears to be efficient in procyclic *T. brucei* (Figure 23A), unlike in the bloodstream form (Figure 11A). RNAi-TbKIFx cells expressing TbKIFx-HA and TbPH1-V5 were split into two cultures: one treated with doxycycline to deplete TbKIFx, and one untreated control. During RNAi induction, the growth of both induced and non-induced cultures (control) was monitored (Figure 22).

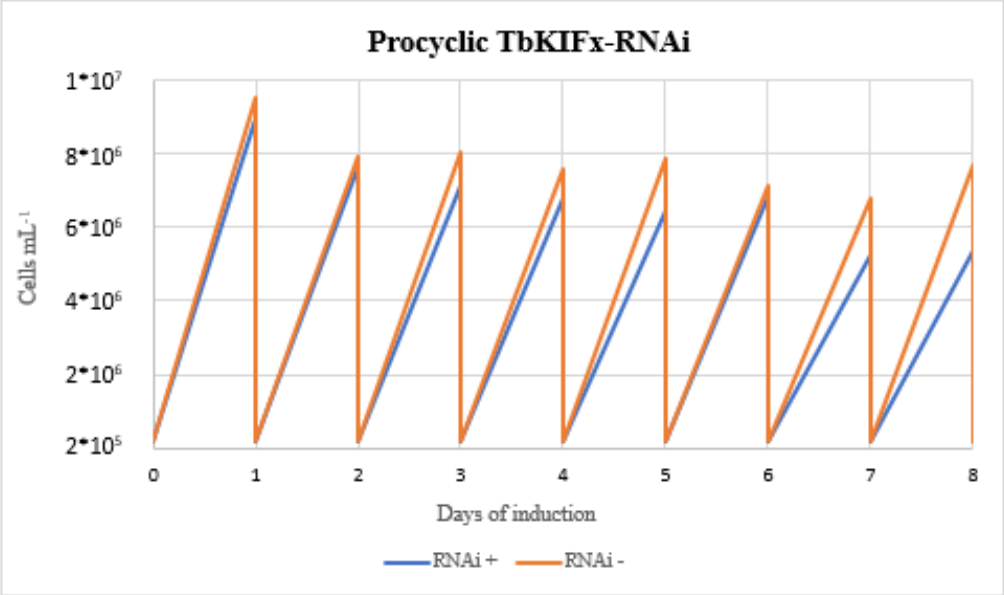

Figure 22: Growth curve of RNAi-induced (blue) and non-induced (orange) procyclic TbKIFx-RNAi cells. Y-axis, cell density; X-axis, days of RNAi induction.

The depletion of TbKIFx did not affect the growth in comparison to non-induced controls of the procyclic cells until day 5 (Figure 22). A consistent growth suppression was observed after day 6, but the decrease was minor.

Western blot analysis revealed the interesting behaviour of TbPH1 upon TbKIFx depletion. TbPH1 remained in the cytosolic fraction upon fully downregulating TbKIFx. Concurrently, TbPH1 was absent in the cytoskeletal fraction of the TbKIFx knockdowns (Figure 23A).

The degree of tyrosine phosphorylation was not significantly affected by the depletion of TbKIFx and the partial depletion of TbPH1 (Figure 23B). The negative control blot that was treated with alkaline phosphatase (see Materials and Methods 3.4.2.5.) exhibited no signal after probing the membrane with the p-Tyr antibody (4G10) (Figure 23C). This confirms that the antibody 4G10 is specific for phosphotyrosine-containing proteins, verifying the western blot shown in Figure 22B. Coomassie blue staining confirms equal loading of protein amounts between the RNAi non-induced and RNAi induced samples within the different fractions (Figure 23D). The occurrence of α-tubulin in the cytosolic fraction indicates incomplete sub-fractionation of the cytoskeleton (Figure 23A). Therefore, the results must be interpreted with caution.

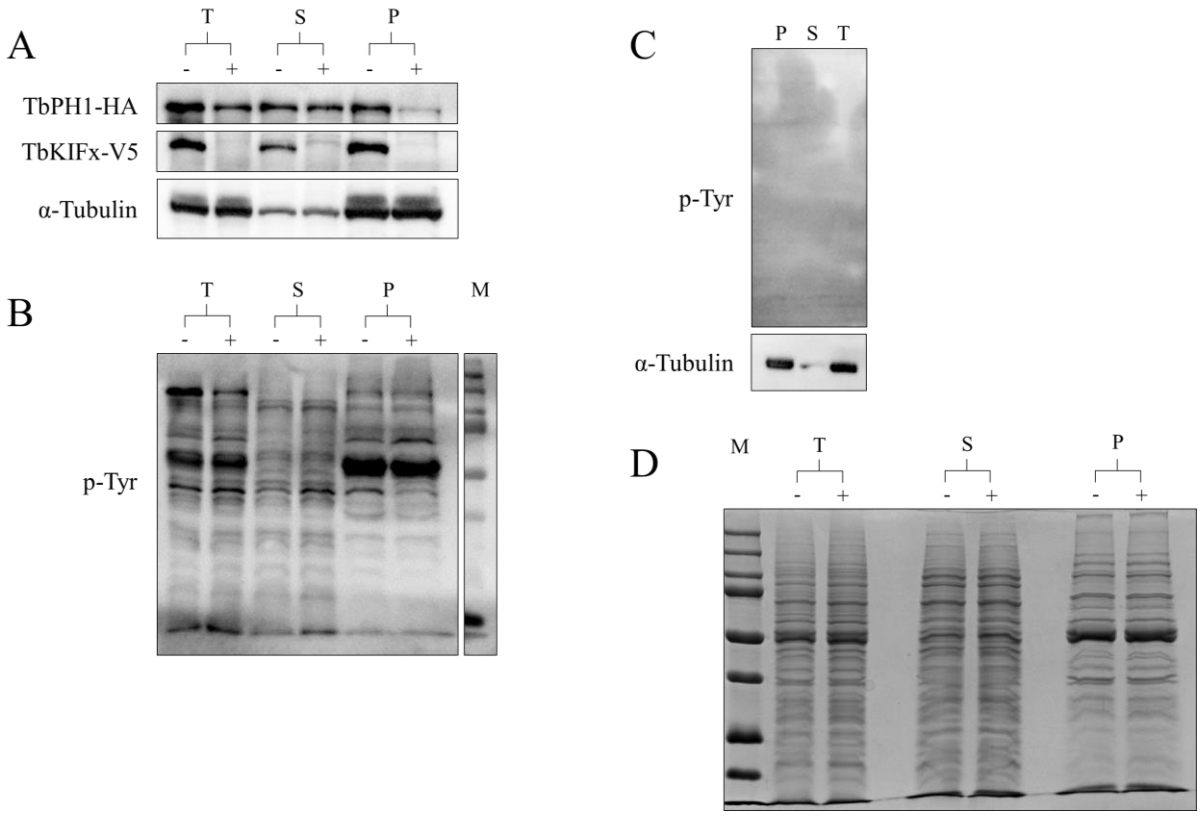

Figure 23: Western blot analysis of MME mediated cytoskeleton fractionation of TbKIFx-RNAi procyclic *T. brucei*. The RNAi induced cultures are indicated by (+) and the non-induced cultures by (-). (T) represents the total cell lysate, (S) the cytoplasmic fraction, (P) the cytoskeletal fraction and (M) the prestained protein ladder. RNAi was induced for 6 days with doxycycline before harvesting. Immunodecorated α-tubulin serves as a cytoskeleton marker. (A) TbKIFx-V5 was fully depleted in every fraction. TbPH1 persisted in the cytosolic fraction (S) and the total cell lyste (T). The cytosolic fraction of induced and non-induced cells contained a certain amount of α-tubulin (B) No significant difference in p-Tyr was detected between RNAi non-induced (-) (control) and RNAi induced (+) cultures. (C) The replicate blot treated with alkaline phosphatase (see Materials and Methods 3.4.2.5.) showed no unspecific binding of the p-Tyr antibody (4G10) (Table VI). (D) The Coomassie blue staining served as loading control.

5. Discussion

In this study, we have identified the localization of TbKIFx and TbPH1 in procyclic and bloodstream *T. brucei* by IFA and western blot analysis. The NP-40 cytoskeleton fractionation of bloodstream SmOx B4 (Figure 12) showed that TbKIFx and TbPH1 are mainly found in the cytoskeletal fraction. However, TbPH1 occurs also in the cytoplasmic fraction, probably needing to be recruited to the cytoskeleton by binding with TbKIFx. A similar result was obtained when analysing the MME cytoskeleton fractionation of procyclic SmOx P9 by western blot (Figure 23A).

IFA analysis of cytoskeleton extractions of bloodstream (Figure 14) and procyclic cells (Figure 18) confirmed the binding of TbKIFx and TbPH1 to the cytoskeleton. Furthermore, these results demonstrated that TbKIFx co-localizes with TbPH1 in both cell cycle stages. Therefore, we conclude that TbKIFx and TbPH1 are associated in bloodstream cells as well in procyclic cells, which agrees with the immunoprecipitation and mass spectrometry data of Kaltenbrunner (2017).

Interestingly, IFAs of procyclic *T. brucei* cytoskeleton extractions revealed that the mBB and MtQ represent potential binding sites of the TbKIFx/TbPH1 dimer. Our investigations demonstrate that immunofluorescent labelled MtQ (Figure 19) and mBB (Figure 20) overlap with the TbPH1 signal in PEME mediated procyclic cytoskeleton structures.

Similar results were obtained in MME mediated cytoskeleton extractions of bloodstream *T. brucei* using IFA. We observed that TbKIFx co-localizes with the immunofluorescent labelled FAZ filaments (Figure 16A) and the mBB (Figure 16B) in cytoskeleton extractions of bloodstream cells. However, TbKIFx exhibited a continuous signal from the mBB to the FAZ filaments. Thus, we hypothesise that TbKIFx/TbPH1 may interact with the MtQ, since it is the only link between the FAZ-filaments and mBB (Vaughan & Gull, 2015). This hypothesis is further supported by the immunogold labelling of tagged TbKIFx on MME cytoskeleton extracted SmOx B4 visualized by SEM (Figure 17). These results showed an enrichment of TbKIFx on a cytoskeleton structure along the flagellum, we believe represents the MtQ (Langousis & Hill, 2014).

It is worth noting that so far only the protein TbSpef1 has been localized to the MtQ (Gheiratmand *et al.,* 2012). Unlike TbKIFx and TbPH1, orthologues of TbSpef1 are present in a wide range of species and probably play an important part of the flagellar structure (Chan *et al*., 2005).

Western blot analysis of knockdowns of TbKIFx in procyclic SmOx P9 revealed that depleting TbKIFx results in a decrease of the TbPH1 steady state. TbPH1 does not fully disappear upon the complete depletion of TbKIFx. While TbPH1 is absent in the cytoskeletal fraction of TbKIFx-RNAi induced cells, a certain amount of the protein remains in the cytoplasm (Figure 23A). This led us to assume that TbPH1 is not able to assemble on the cytoskeleton without TbKIFx. However, it is very unlikely that TbPH1 operates independently from TbKIFx in the cytoplasm of *T. brucei*, due to the co-localization of TbKIFx and TbPH1 in whole cell IFA (Figure 13).

Like many other cytoskeleton proteins and proteins regulating the cytoskeleton (Lemmon *et al.*, 2001), TbPH1 contains also a PH-domain, which may enable the binding or interaction with tyrosine-phosphorylated proteins (Scheffzek & Welti, 2012). Our IFA data revealed that cytoskeleton associated tyrosine-phosphorylated proteins co-localize with TbKIFx/TbPH1 in bloodstream *T. brucei* (Figure 21). However, immunoblot analysis of procyclic SmOx P9 expressing RNAi-TbKIFx showed no conclusive effect on the degree of tyrosine-phosphorylated proteins (Figure 23B). This result does not necessarily disprove our hypothesis that TbKIFx/TbPH1 interact with tyrosine-phosphorylated proteins. There are several possible explanations for this result. First, TbKIFx-knockdown may not affect the steady state levels of tyrosine-phosphorylated proteins. Second, depletion of TbKIFx may affect only a small extent of tyrosine-phosphorylated proteins. Small changes of non-abundant tyrosine-phosphorylated proteins are not detectable using an assay based upon immunodetection of p-Tyr on western blots (Nett *et al.*, 2009). Finally, TbKIFx/TbPH1 may not interact with tyrosine-phosphorylated proteins and therefore rejecting our hypothesis.

6. Conclusion

In this study we have shown that the kinesin TbKIFx and the kinesin-like TbPH1 interact in bloodstream and procyclic *T. brucei* using IFA. Considerable process has been made with regard to the localization of TbKIFx/TbPH1. We found that TbKIFx/TbPH1 probably bind to the mBB and MtQ in both life cycle stages. Similar findings were obtained by investigating the localization of TbKIFx in cytoskeleton extractions of bloodstream *T. brucei* using SEM.

Also, notable insight has been gained with regard to the interaction of TbKIFx and TbPH1 using TbKIFx-knockdowns. Depletion of TbKIFx in procyclic cells hindered TbPH1 assembly on the cytoskeleton and resulted in a decrease of TbPH1 steady state in whole cells.

Moreover, we demonstrated that TbKIFx/TbPH1 co-localize with cytoskeleton associated tyrosine-phosphorylated proteins by IFA. However, the performed western blot on TbKIFx-RNAi cell lines did not show any conclusive effect on the degree of tyrosine-phosphorylated proteins.

7. Future perspectives

Further work needs to be done to better establish whether TbKIFx/TbPH1 binds to the MtQ. It is impossible to distinguish between the MtQ and FAZ filaments using the fluorescent microscope Axioplane 2 (Zeiss). Thus, we plan to visualize TbPH1 and TbKIFx in transverse sections by transmission electron microscopy (TEM). We attempt to immunogold-label TbPH1/TbKIFx and look for enrichments of the gold nanoparticles in the MtQ, which can be identified by being surrounded by ER (Sunter & Gull, 2016).

In addition, we consider stimulated emission depletion (STED) microscopy to confirm the interaction of TbKIFx/TbPH1 with the mBB and MtQ in PEME mediated cytoskeleton extractions of both *T.brucei* life cycle stages by IFA (Westphal *et al.*, 2008; Vicidomini *et al.*, 2018). STED provides super-resolution images by reversibly silencing fluorophores, which are not located in the focal point. Only fluorophores that are within the focal area are not silenced and emit light upon excitation. This reduces the area of illumination and consequently enhances the resolution (Westphal *et al.*, 2008).

We intend to repeat immunoblot experiments of both life cycle stages using the PEME buffer. By using the PEME buffer, we expect to enhance the completeness of the fractionation and therefore, minimize the α-tubulin contamination in the soluble fraction. This should give us a more accurate result about the distribution of TbPH1 and TbKIFx between the cytoskeletal and cytoplasmic fraction.

A more accurate approach to resolve the potential cargo of TbKIFx/TbPH1 is the BioID method, which is based on cellular biotinylating of proximal proteins using a promiscuous biotin ligase (Kim *et al.*, 2016). The protein of interest TbPH1 is fused with the biotin ligase, which biotinylates proximal endogenous proteins (Roux *et al.*, 2018). The reason why the application is so successful is that biotinylation is a rare protein modification in nature. Thus, proteins that are biotinylated during this process are easily identified (Roux *et al.*, 2018).
The method consists of three stages: (1) the generation of cell lines expressing the BioID fused protein, (2) the induction of biotinylation and (3) large-scale BioID pull-down to identify the protein candidates by mass spectrometry (Roux *et al.*, 2018).
(1) We assume that the PH-domain of TbPH1 represents the binding site of potential cargos of the TbKIFx/TbPH1 dimer. Therefore, we plan to create procyclic cell lines expressing

TbPH1-HA fused with the biotin ligase by electroporation with the respective DNA vector (Roux *et al.*, 2018).

(2) After the generation of the cell line expressing TbPH1-BioID2, biotinylation is induced by the addition of excess biotin into the media (Roux *et al.*, 2018).

(3) Biotinylated proteins are purified by streptavidin-mediated pull down and send to mass spectrometry analysis, which enables the identification of potential cargo candidates of TbKIFx/TbPH1 (Li *et al.*, 2018)

8. References

Adl, S. M. *et al*. (2018). Revisions to the Classification, Nomenclature, and Diversity of Eukaryotes. Journal of Eukaryotic Microbiology. https://doi.org/10.1111/jeu.12691

Alberts, B. *et al.* (2002). Molecular Biology of the Cell. 4th edition. New York: Garland Science. Molecular Motors. Retrieved from https://www.ncbi.nlm.nih.gov/books/NBK21054/

Autrata, R. (1992) Single crystal detector suitable for high resolution scanning electron microscopy. EMSA Bull. 22, 54 – 58

Balmer, O., Beadell, J. S., Gibson, W., & Caccone, A. (2011). Phylogeography and Taxonomy of *Trypanosoma brucei*. PLoS Neglected Tropical Diseases, 5(2), e961. https://doi.org/10.1371/journal.pntd.0000961

Bray, D. F., Bagu, J., & Koegler, P. (1993). Comparison of hexamethyldisilazane (HMDS), Peldri II, and critical-point drying methods for scanning electron microscopy of biological specimens. Microscopy Research and Technique, 26(6), 489–495. https://doi.org/10.1002/jemt.1070260603

Brun, R. & Schonenberger, M. (1979). Cultivation and *in vitro* cloning or procyclic culture forms of *Trypanosoma brucei* in a semi-defined medium. Short communication. Acta Trop, 36, 289-292.

Chan, S. W., Fowler, K. J., Choo, K. H. A., & Kalitsis, P. (2005). Spef1, a conserved novel testis protein found in mouse sperm flagella. Gene, 353(2), 189–199. https://doi.org/10.1016/j.gene.2005.04.025

Concepción-Acevedo, J., Luo, J., & Klingbeil, M. M. (2012). Dynamic Localization of *Trypanosoma brucei* Mitochondrial DNA Polymerase ID. Eukaryotic Cell, 11(7), 844–855. https://doi.org/10.1128/EC.05291-11

Dean, S. *et al.* (2015). A toolkit enabling efficient, scalable and reproducible gene tagging in trypanosomatids. Open Biology, 5(1), 140197. https://doi.org/10.1098/rsob.140197

Esson, H. J. *et al.* (2012). Morphology of the Trypanosome Bilobe, a Novel Cytoskeletal Structure. Eukaryotic Cell, 11(6), 761–772. https://doi.org/10.1128/EC.05287-11

Field, M. C., & Carrington, M. (2009). The trypanosome flagellar pocket. Nature Reviews Microbiology, 7(11), 775–786. https://doi.org/10.1038/nrmicro2221

Gallo, J.-M., Précigout, E., & Schrével, J. (1988). Subcellular sequestration of an antigenically unique β-tubulin. Cell Motility and the Cytoskeleton, 9(2), 175–183. https://doi.org/10.1002/cm.970090209

Gheiratmand, L., Brasseur, A., Zhou, Q., & He, C. Y. (2012). Biochemical Characterization of the Bi-lobe Reveals a Continuous Structural Network Linking the Bi-lobe to Other Single-copied Organelles in *Trypanosoma brucei*. Journal of Biological Chemistry, 288(5), 3489–3499. https://doi.org/10.1074/jbc.m112.417428

Hampl, V. *et al.* (2009). Phylogenomic analyses support the monophyly of Excavata and resolve relationships among eukaryotic "supergroups." Proceedings of the National Academy of Sciences, 106(10), 3859–3864. https://doi.org/10.1073/pnas.0807880106

Hemphill, A., Lawson, D., & Seebeck, T. (1991). The Cytoskeletal Architecture of *Trypanosoma brucei*. The Journal of Parasitology, 77(4), 603. https://doi.org/10.2307/3283167

Hirokawa, N., Noda, Y., Tanaka, Y., & Niwa, S. (2009). Kinesin superfamily motor proteins and intracellular transport. Nature Reviews Molecular Cell Biology, 10(10), 682–696. https://doi.org/10.1038/nrm2774

Hirose, K., Akimaru, E., Akiba, T., Endow, S. A., & Amos, L. A. (2006). Large Conformational Changes in a Kinesin Motor Catalyzed by Interaction with Microtubules. Molecular Cell, 23(6), 913–923. https://doi.org/10.1016/j.molcel.2006.07.020

Hirumi, H., & Hirumi, K. (1989). Continuous Cultivation of *Trypanosoma brucei* Blood Stream Forms in a Medium Containing a Low Concentration of Serum Protein without Feeder Cell Layers. The Journal of Parasitology, 75(6), 985. https://doi.org/10.2307/3282883

Höög, J. L., Bouchet-Marquis, C., McIntosh, J. R., Hoenger, A., & Gull, K. (2012). Cryo-electron tomography and 3-D analysis of the intact flagellum in *Trypanosoma brucei*. Journal of Structural Biology, 178(2), 189–198. https://doi.org/10.1016/j.jsb.2012.01.009

Hu, L., Hu, H., & Li, Z. (2012). A kinetoplastid-specific kinesin is required for cytokinesis and for maintenance of cell morphology in *Trypanosoma brucei*. Molecular Microbiology, 83(3), 565–578. https://doi.org/10.1111/j.1365-2958.2011.07951.x

Kaltenbrunner, S. (2017, April 18). Characterization of TbPH1, a kinetoplastid-specific pleckstrin homology domain containing kinesin-like protein. Retrieved from https://theses.cz/id/wo6l3c/

Kaurov, I. *et al.* (2018). The Diverged Trypanosome MICOS Complex as a Hub for Mitochondrial Cristae Shaping and Protein Import. Current Biology, 28(21), 3393-3407.e5. https://doi.org/10.1016/j.cub.2018.09.008

Kilmartin, J. V. (1982). Rat monoclonal antitubulin antibodies derived by using a new nonsecreting rat cell line. The Journal of Cell Biology, 93(3), 576–582. https://doi.org/10.1083/jcb.93.3.576

Kim, D. I. *et al.* 2016). An improved smaller biotin ligase for BioID proximity labeling. Molecular Biology of the Cell, 27(8), 1188–1196. https://doi.org/10.1091/mbc.E15-12-0844

Kohl, L., & Gull, K. (1998). Molecular architecture of the trypanosome cytoskeleton. Molecular and Biochemical Parasitology, 93(1), 1–9. https://doi.org/10.1016/s0166-6851(98)00014-0

Kohl, L., Sherwin, T., & Gull, K. (1999). Assembly of the Paraflagellar Rod and the Flagellum Attachment Zone Complex During the *Trypanosoma brucei* Cell Cycle. The Journal of Eukaryotic Microbiology, 46(2), 105–109. https://doi.org/10.1111/j.1550-7408.1999.tb04592.x

Lacomble, S., Vaughan, S., Deghelt, M., Moreira-Leite, F. F., & Gull, K. (2012). A *Trypanosoma brucei* Protein Required for Maintenance of the Flagellum Attachment Zone and Flagellar Pocket ER Domains. Protist, 163(4), 602–615. https://doi.org/10.1016/j.protis.2011.10.010

Langousis, G., & Hill, K. L. (2014). Motility and more: the flagellum of *Trypanosoma brucei*. Nature Reviews Microbiology, 12(7), 505–518. https://doi.org/10.1038/nrmicro3274

Lemmon, M. A., Ferguson, K. M., & Abrams, C. S. (2001). Pleckstrin homology domains and the cytoskeleton. FEBS Letters, 513(1), 71–76. https://doi.org/10.1016/s0014-5793(01)03243-4

Li, P., Meng, Y., Wang, L., & Di, L. (2018). BioID: A Proximity-Dependent Labeling Approach in Proteomics Study. Functional Proteomics, 143–151. https://doi.org/10.1007/978-1-4939-8814-3_10

Lucanus, A. J., & Yip, G. W. (2017). Kinesin superfamily: roles in breast cancer, patient prognosis and therapeutics. Oncogene, 37(7), 833–838. https://doi.org/10.1038/onc.2017.406

Matthews, K. R. (2005). The developmental cell biology of *Trypanosoma brucei*. Journal of Cell Science, 118(2), 283–290. https://doi.org/10.1242/jcs.01649

McAllaster, M. R., Sinclair-Davis, A. N., Hilton, N. A., & de Graffenried, C. L. (2016). A unified approach towards *Trypanosoma brucei* functional genomics using Gibson assembly. Molecular and Biochemical Parasitology, 210(1–2), 13–21. https://doi.org/10.1016/j.molbiopara.2016.08.001

Montagnes, D., Roberts, E., Lukeš, J., & Lowe, C. (2012). The rise of model protozoa. Trends in Microbiology, 20(4), 184–191. https://doi.org/10.1016/j.tim.2012.01.007

Nett, I. R. E., Davidson, L., Lamont, D., & Ferguson, M. A. J. (2009). Identification and Specific Localization of Tyrosine-Phosphorylated Proteins in *Trypanosoma brucei*. Eukaryotic Cell, 8(4), 617–626. https://doi.org/10.1128/EC.00366-08

Poon, S. K., Peacock, L., Gibson, W., Gull, K., & Kelly, S. (2012). A modular and optimized single marker system for generating *Trypanosoma brucei* cell lines expressing T7 RNA polymerase and the tetracycline repressor. Open Biology, 2(2), 110037. https://doi.org/10.1098/rsob.110037

Ralston, K. S., & Hill, K. L. (2008). The flagellum of *Trypanosoma brucei*: New tricks from an old dog. International Journal for Parasitology, 38(8–9), 869–884. https://doi.org/10.1016/j.ijpara.2008.03.003

Rice, S. *et al*. (1999). A structural change in the kinesin motor protein that drives motility. Nature, 402(6763), 778–784. https://doi.org/10.1038/45483

Roux, K. J., Kim, D. I., Burke, B., & May, D. G. (2018). BioID: A Screen for Protein-Protein Interactions. Current Protocols in Protein Science, 91(1). https://doi.org/10.1002/cpps.51

Sablin, E. P. (2000). Kinesins and microtubules: their structures and motor mechanisms. Current Opinion in Cell Biology, 12(1), 35–41. https://doi.org/10.1016/s0955-0674(99)00054-x

Saraste, M., Sibbald, P. R., & Wittinghofer, A. (1990). The P-loop — a common motif in ATP- and GTP-binding proteins. Trends in Biochemical Sciences, 15(11), 430–434. https://doi.org/10.1016/0968-0004(90)90281-f

Scheffzek, K., & Welti, S. (2012). Pleckstrin homology (PH) like domains - versatile modules in protein-protein interaction platforms. FEBS Letters, 586(17), 2662–2673. https://doi.org/10.1016/j.febslet.2012.06.006

Schneider, A., Hemphill, A., Wyler, T., & Seebeck, T. (1988). Large microtubule-associated protein of *T. brucei* has tandemly repeated, near-identical sequences. Science, 241(4864), 459–462. https://doi.org/10.1126/science.3393912

Shaw, G. (1996). The pleckstrin homology domain: An intriguing multifunctional protein module. BioEssays, 18(1), 35–46. https://doi.org/10.1002/bies.950180109

Sunter, J. D., & Gull, K. (2016). The Flagellum Attachment Zone: 'The Cellular Ruler' of Trypanosome Morphology. Trends in Parasitology, 32(4), 309–324. https://doi.org/10.1016/j.pt.2015.12.010

Trikin, R. *et al.* (2016). TAC102 Is a Novel Component of the Mitochondrial Genome Segregation Machinery in Trypanosomes. PLOS Pathogens, 12(5), e1005586. https://doi.org/10.1371/journal.ppat.1005586

Vaughan, S., & Gull, K. (2015). Basal body structure and cell cycle-dependent biogenesis in *Trypanosoma brucei*. Cilia, 5(1). https://doi.org/10.1186/s13630-016-0023-7

Vaughan, S., Kohl, L., Ngai, I., Wheeler, R. J., & Gull, K. (2008). A Repetitive Protein Essential for the Flagellum Attachment Zone Filament Structure and Function in *Trypanosoma brucei*. Protist, 159(1), 127–136. https://doi.org/10.1016/j.protis.2007.08.005

Vicidomini, G., Bianchini, P., & Diaspro, A. (2018). STED super-resolved microscopy. Nature Methods, 15(3), 173–182. https://doi.org/10.1038/nmeth.4593

Westphal, V. *et al.* (2008). Video-Rate Far-Field Optical Nanoscopy Dissects Synaptic Vesicle Movement. Science, 320(5873), 246–249. https://doi.org/10.1126/science.1154228

Wickstead, B., & Gull, K. (2006). A "Holistic" Kinesin Phylogeny Reveals New Kinesin Families and Predicts Protein Functions. Molecular Biology of the Cell, 17(4), 1734–1743. https://doi.org/10.1091/mbc.E05-11-1090